

GRAVITATIONAL ENCOUNTERS AND THE EVOLUTION OF GALACTIC NUCLEI. I. METHOD

DAVID MERRITT

School of Physics and Astronomy and Center for Computational Relativity and Gravitation, Rochester Institute of Technology,
Rochester, NY 14623

Draft version June 9, 2021

ABSTRACT

An algorithm is described for evolving the phase-space density of stars or compact objects around a massive black hole at the center of a galaxy. The technique is based on numerical integration of the Fokker-Planck equation in energy-angular momentum space, $f(E, L, t)$, and includes, for the first time, diffusion coefficients that describe the effects of both random and correlated encounters (“resonant relaxation”), as well as energy loss due to emission of gravitational waves. Destruction or loss of stars into the black hole are treated by means of a detailed boundary-layer analysis. Performance of the algorithm is illustrated by calculating two-dimensional, time-dependent and steady-state distribution functions and their corresponding loss rates.

Subject headings: galaxies: evolution — galaxies: kinematics and dynamics — galaxies: nuclei

1. INTRODUCTION

The distribution of stars around a massive black hole is a well-studied problem. Many solutions are consistent with Jeans’s theorem, but after a sufficiently long time, gravitational encounters between stars will drive their distribution toward a predictable form. In the case of stars of a single mass, random encounters result in a steady-state distribution that was first correctly described by Bahcall and Wolf (1976): the density of stars falls off as $n(r) \propto r^{-7/4}$, and the phase-space density is $f(E) \propto |E|^{1/4}$; here r is distance from the black hole and E is the orbital energy per unit mass of a star. Bahcall and Wolf’s derivation assumed that the gravitational potential was dominated by the black hole, and that the distribution of stars in velocity space was isotropic. Capture of stars by the hole was allowed to occur only via diffusion in energy; the steady-state feeding rate was found to be small, in the sense that a small fraction of stars, within any radius, are consumed by the hole in one, two-body relaxation time at that radius. For this reason, $f \sim |E|^{1/4}$ is often described as a “zero flux” solution and in fact it can most easily be derived by setting to zero the energy-space flux in the evolution equation for the orbital distribution.

Frank & Rees (1976) argued that feeding of the black hole would be dominated by diffusion in angular momentum, not energy, and that a fraction of order unity of stars within radius r would be captured in one relaxation time at r . Lightman & Shapiro (1977) and Cohn & Kulsrud (1978) found steady-state solutions of the equations describing diffusion in both E and L ; capture or destruction of stars was assumed to occur when the orbital eccentricity was large enough, at a given energy, that the orbit intersected the loss sphere, the region around the hole in which stars are consumed or tidally disrupted. The steady-state solutions found by these authors were anisotropic with respect to velocity, since the phase space density must be zero near the loss sphere. However the steady-state energy distribution was found to be quite similar to that of the scale-free Bahcall-Wolf solution, at least for energies much greater than that of a circular orbit at the edge of the capture sphere, and the corresponding configuration-space density was close to $n \sim r^{-7/4}$ outside of this sphere.

These early treatments were made possible by the availability of analytic expressions for the diffusion coefficients that describe encounter-driven changes in E and L . Such expressions can be straightforwardly derived in the case of random encounters in a homogeneous medium (e.g. Rosenbluth et al. 1957; Cohn & Kulsrud 1978). Sufficiently near to a massive black hole – very roughly, at distances less than $\sim 10^{-1}$ times the black hole’s gravitational influence radius – the assumption of random encounters breaks down, since orbits resemble closed Keplerian ellipses for many periods. In this regime, diffusion in angular momentum is dominated by “resonant relaxation” (RR) (Rauch & Tremaine 1996) while changes in energy are still controlled by random (“non-resonant,” NR) encounters. Approximate timescales for changes in L in the RR regime have long been available, but until recently, usefully accurate expressions for the diffusion coefficients in L were not available. Happily, that situation has now begun to change (Hamers, Portegies Zwart & Merritt 2014), and so it is feasible to repeat calculations like those of Cohn & Kulsrud (1978) using expressions for the diffusion coefficients that are valid much closer to the black hole.

This paper, which is the first in a series, presents a numerical algorithm for solving the Fokker-Planck equation describing the evolution due to gravitational encounters of $f(E, L)$, the two-dimensional phase-space density of stars orbiting around a massive black hole. The basic numerical approach is the same as that of Cohn & Kulsrud (1978), although their algorithm has been generalized to include diffusion coefficients that describe both random and correlated encounters. Cohn & Kulsrud’s treatment is improved upon in other ways as well; notably by the use of a logarithmic grid in angular momentum, which is necessary to accurately treat the behavior of highly eccentric orbits.

As far as we are aware, the time-dependent, $f(E, L, t)$ solutions presented here are the first ever published. While Cohn & Kulsrud’s algorithm was capable of calculating time-dependent solutions, those authors (perhaps because of computer limitations) chose to present only steady-state solutions in their 1978 paper. Time dependence is particularly relevant to galactic nuclei since (energy) relaxation times are believed to be comparable with galaxy lifetimes, even in nuclei as dense as that of the Milky Way (Merritt 2010). This time dependence has routinely been ignored in calculations of the rate of stellar tidal disruptions (e.g. Magorrian & Tremaine 1998).

In spite of the improvements, the algorithm presented here still contains some basic limitations. The mass of the black hole is fixed and its spin is ignored. Stars are assumed to have a single mass, and the contribution of the stars to the gravitational potential is ignored. As a consequence, results are limited in their applicability to a region inside the black hole’s sphere of gravitational influence, and the possible influence of spatial asymmetries in the stellar potential on the behavior of orbits is ignored. There is no “source term” corresponding to star formation and binary stars are not allowed. Rotation of the stellar cluster is ignored. Some of these restrictions will be lifted in later papers from this series.

2. ASSUMPTIONS AND BASIC RELATIONS

Stars – a term used here to refer both to normal stars and to compact objects, e.g. stellar-mass black holes – are assumed to have a single mass, m_* . The stars are assumed to be close enough to the black hole (SBH) that the gravitational potential defining their unperturbed orbits is constant in time and given by

$$\Phi(r) \equiv -\psi(r) = -\frac{GM_\bullet}{r} \quad (1)$$

with M_\bullet the SBH mass, also assumed constant. The contribution to the potential from the stars themselves is ignored, hence results are only expected to be accurate inside the SBH gravitational influence sphere.

Unperturbed orbits respect the two isolating integrals E (energy) and L (angular momentum), both defined per unit mass:

$$E = \frac{v^2}{2} + \Phi(r) = \frac{v^2}{2} - \frac{GM_\bullet}{r}, \quad L = |\mathbf{r} \times \mathbf{v}|. \quad (2)$$

Following Cohn & Kulsrud (1978) we define new variables $(\mathcal{E}, \mathcal{R})$ as

$$\mathcal{E} \equiv -E = -\frac{v^2}{2} + \psi(r), \quad \mathcal{R} \equiv \frac{L^2}{L_c^2} \quad (3)$$

with $L_c(\mathcal{E})$ the angular momentum of a circular orbit of energy \mathcal{E} :

$$L_c^2(\mathcal{E}) = \frac{(GM_\bullet)^2}{2\mathcal{E}}. \quad (4)$$

Hence $0 \leq \mathcal{R} \leq 1$. \mathcal{E} and \mathcal{R} are related to the semimajor axis a and eccentricity e of the Keplerian orbit via

$$a = \frac{GM_\bullet}{2\mathcal{E}}, \quad e^2 = 1 - \mathcal{R}. \quad (5)$$

The orbital (Kepler) period is

$$P(a) = \frac{2\pi a^{3/2}}{\sqrt{GM_\bullet}} = \frac{\pi}{\sqrt{2}} \frac{GM_\bullet}{\mathcal{E}^{3/2}} \quad (6)$$

and the gravitational radius of the SBH is

$$r_g \equiv \frac{GM_\bullet}{c^2} \approx 4.80 \times 10^{-5} \left(\frac{M_\bullet}{10^6 M_\odot} \right) \text{ mpc}. \quad (7)$$

Spin of the SBH is ignored.

Stars are assumed to be lost – either captured, or destroyed – if their (Newtonian) periapsis distance falls below r_{1c} , i.e. if

$$a(1 - e) \leq r_{1c}. \quad (8)$$

For stars not subject to tidal disruption, e.g. compact objects, $r_{1c} \approx 8r_g$ (Merritt 2013, §4.6); otherwise $r_{1c} > 8r_g$ is the tidal disruption radius. Defining

$$\mathcal{E}_{1c} \equiv \frac{GM_\bullet}{2r_{1c}}, \quad (9)$$

the energy of a circular orbit at $r = r_{1c}$, allows the loss condition to be written as

$$\mathcal{R} \leq \mathcal{R}_{1c}(\mathcal{E}) = 2 \frac{\mathcal{E}}{\mathcal{E}_{1c}} \left(1 - \frac{1}{2} \frac{\mathcal{E}}{\mathcal{E}_{1c}} \right), \quad \mathcal{E} \leq \mathcal{E}_{1c}. \quad (10)$$

For $\mathcal{E} \ll \mathcal{E}_{\text{lc}}$, equations (9) and (10) imply

$$\mathcal{R}_{\text{lc}} \approx 2 \frac{\mathcal{E}}{\mathcal{E}_{\text{lc}}} \approx 32 \frac{\mathcal{E}}{c^2}; \quad (11)$$

the final expression assumes $\mathcal{E}_{\text{lc}} = c^2/16$, appropriate for $r_{\text{lc}} = 8r_g$.

The number density of stars in phase space, f , is assumed to satisfy Jeans's theorem at any given time, but the dependence of f on \mathcal{E} and \mathcal{R} is allowed to vary with time as gravitational encounters cause stars to change their orbits:

$$f = f(\mathcal{E}, \mathcal{R}, t). \quad (12)$$

The configuration-space density is given in terms of f as

$$n(r) = \frac{2\pi}{r^2} \int_0^{\psi(r)} L_c^2(\mathcal{E}) d\mathcal{E} \int_0^{\mathcal{R}_{\text{max}}} \frac{f(\mathcal{E}, \mathcal{R}) d\mathcal{R}}{\sqrt{2[\psi(r) - \mathcal{E}] - \mathcal{R}L_c^2(\mathcal{E}, t)/r^2}} \quad (13a)$$

$$= \sqrt{2\pi} \frac{GM_\bullet}{r} \int_0^{GM_\bullet/r} \frac{d\mathcal{E}}{\sqrt{\mathcal{E}}} \int_0^{\mathcal{R}_{\text{max}}} \frac{f(\mathcal{E}, \mathcal{R}, t) d\mathcal{R}}{\sqrt{\mathcal{R}_{\text{max}} - \mathcal{R}}} \quad (13b)$$

where

$$\mathcal{R}_{\text{max}}(\mathcal{E}, r) = \frac{2r^2[\psi(r) - \mathcal{E}]}{L_c^2(\mathcal{E})} = 4 \left(\frac{r\mathcal{E}}{GM_\bullet} \right) \left(1 - \frac{r\mathcal{E}}{GM_\bullet} \right) \quad (14)$$

with similar expressions for the velocity dispersions σ_r, σ_t in the radial and transverse directions.

The time dependence of f is assumed to be described by the orbit-averaged Fokker-Planck equation:

$$\frac{\partial N}{\partial t} = -\frac{\partial}{\partial \mathcal{E}} (N \langle \Delta \mathcal{E} \rangle_t) + \frac{1}{2} \frac{\partial^2}{\partial \mathcal{E}^2} (N \langle (\Delta \mathcal{E})^2 \rangle_t) - \frac{\partial}{\partial \mathcal{R}} (N \langle \Delta \mathcal{R} \rangle_t) + \frac{1}{2} \frac{\partial^2}{\partial \mathcal{R}^2} (N \langle (\Delta \mathcal{R})^2 \rangle_t) + \frac{\partial^2}{\partial \mathcal{E} \partial \mathcal{R}} (N \langle \Delta \mathcal{E} \Delta \mathcal{R} \rangle_t) \quad (15)$$

where

$$N(\mathcal{E}, \mathcal{R}, t) = 4\pi^2 L_c^2(\mathcal{E}) P(\mathcal{E}, \mathcal{R}) f(\mathcal{E}, \mathcal{R}, t) = \sqrt{2}\pi^3 (GM_\bullet)^3 \mathcal{E}^{-5/2} f(\mathcal{E}, \mathcal{R}, t) \equiv \mathcal{J}(\mathcal{E}, \mathcal{R}) f(\mathcal{E}, \mathcal{R}, t) \quad (16)$$

is the distribution of orbital integrals. The quantities in $\langle \rangle$ in equation (15) are diffusion coefficients; the subscript “ t ” indicates a time average over the unperturbed orbit. The diffusion coefficients are functions of \mathcal{E} , \mathcal{R} and of the stellar distribution itself, i.e. of f ; their functional forms are discussed in more detail below.

Equation (15) can be written in flux-conservation form as (Cohn & Kulsrud 1978)

$$\begin{aligned} \mathcal{J} \frac{\partial f}{\partial t} &= -\frac{\partial}{\partial \mathcal{E}} (\mathcal{J} \phi_{\mathcal{E}}) - \mathcal{J} \frac{\partial}{\partial \mathcal{R}} \phi_{\mathcal{R}} \\ -\phi_{\mathcal{E}} &= D_{\mathcal{E}\mathcal{E}} \frac{\partial f}{\partial \mathcal{E}} + D_{\mathcal{E}\mathcal{R}} \frac{\partial f}{\partial \mathcal{R}} + D_{\mathcal{E}} f, \\ -\phi_{\mathcal{R}} &= D_{\mathcal{R}\mathcal{E}} \frac{\partial f}{\partial \mathcal{E}} + D_{\mathcal{R}\mathcal{R}} \frac{\partial f}{\partial \mathcal{R}} + D_{\mathcal{R}} f \end{aligned} \quad (17)$$

with “flux coefficients”

$$\begin{aligned} D_{\mathcal{E}} &= -\langle \Delta \mathcal{E} \rangle_t - \frac{5}{4\mathcal{E}} \langle (\Delta \mathcal{E})^2 \rangle_t + \frac{1}{2} \frac{\partial}{\partial \mathcal{E}} \langle (\Delta \mathcal{E})^2 \rangle_t + \frac{1}{2} \frac{\partial}{\partial \mathcal{R}} \langle \Delta \mathcal{E} \Delta \mathcal{R} \rangle_t, \\ D_{\mathcal{R}} &= -\langle \Delta \mathcal{R} \rangle_t - \frac{5}{4\mathcal{E}} \langle \Delta \mathcal{E} \Delta \mathcal{R} \rangle_t + \frac{1}{2} \frac{\partial}{\partial \mathcal{E}} \langle \Delta \mathcal{E} \Delta \mathcal{R} \rangle_t + \frac{1}{2} \frac{\partial}{\partial \mathcal{R}} \langle (\Delta \mathcal{R})^2 \rangle_t, \\ D_{\mathcal{E}\mathcal{E}} &= \frac{1}{2} \langle (\Delta \mathcal{E})^2 \rangle_t, D_{\mathcal{E}\mathcal{R}} = D_{\mathcal{R}\mathcal{E}} = \frac{1}{2} \langle \Delta \mathcal{E} \Delta \mathcal{R} \rangle_t, D_{\mathcal{R}\mathcal{R}} = \frac{1}{2} \langle (\Delta \mathcal{R})^2 \rangle_t. \end{aligned} \quad (18)$$

The rate of loss of stars past the loss-cone boundary:

$$\mathcal{R} = \mathcal{R}_{\text{lc}}(\mathcal{E}), \quad \mathcal{E}_{\text{min}} \leq \mathcal{E} \leq \mathcal{E}_{\text{max}} \quad (19)$$

is given in terms of the fluxes as

$$\dot{N} = \int_{\mathcal{E}_{\text{min}}}^{\mathcal{E}_{\text{max}}} d\mathcal{E} \int_{\mathcal{R}_{\text{lc}}(\mathcal{E})}^1 \mathcal{J} \frac{\partial f}{\partial t} d\mathcal{R} = - \int_{\mathcal{E}_{\text{min}}}^{\mathcal{E}_{\text{max}}} d\mathcal{E} \int_{\mathcal{R}_{\text{lc}}(\mathcal{E})}^1 \left[\frac{\partial}{\partial \mathcal{E}} (\mathcal{J} \phi_{\mathcal{E}}) + \mathcal{J} \frac{\partial}{\partial \mathcal{R}} \phi_{\mathcal{R}} \right] \quad (20a)$$

$$= \int_{\mathcal{E}_{\text{min}}}^{\mathcal{E}_{\text{max}}} \mathcal{J}(\mathcal{E}) \phi_{\mathcal{R}}[\mathcal{E}, \mathcal{R}_{\text{lc}}(\mathcal{E})] d\mathcal{E} - \int_{\mathcal{R}_{\text{min}}}^1 \mathcal{J}(\mathcal{E}_{\text{lc}}) \phi_{\mathcal{E}}[\mathcal{E}_{\text{lc}}(\mathcal{R}), \mathcal{R}] d\mathcal{R}. \quad (20b)$$

In the final expression, $\mathcal{R}_{\text{min}} \equiv \mathcal{R}_{\text{lc}}(\mathcal{E}_{\text{min}})$ and \mathcal{E}_{lc} is the value of \mathcal{E} satisfying $\mathcal{R} = \mathcal{R}_{\text{lc}}(\mathcal{E})$. We expect the first of the two terms in (20b) (flux due to diffusion in L) to dominate the loss rate.

A quantity that plays an important role in the angular momentum diffusion of orbits near the loss-cone boundary is

$$\mathcal{D}(\mathcal{E}) \equiv \lim_{\mathcal{R} \rightarrow 0} \frac{\langle (\Delta \mathcal{R})^2 \rangle_t}{2\mathcal{R}} = \lim_{\mathcal{R} \rightarrow 0} \frac{D_{\mathcal{R}\mathcal{R}}(\mathcal{E}, \mathcal{R})}{\mathcal{R}}. \quad (21)$$

In this limit, and ignoring diffusion in \mathcal{E} , the Fokker-Planck equation becomes

$$\frac{\partial N}{\partial (\mathcal{D}t)} \approx \frac{\partial}{\partial \mathcal{R}} \left(\mathcal{R} \frac{\partial N}{\partial \mathcal{R}} \right) \quad (22)$$

showing that \mathcal{D}^{-1} is effectively an orbit-averaged, angular momentum relaxation time at energy \mathcal{E} . Another quantity that can be expressed in terms of \mathcal{D} is

$$q_{\text{lc}}(\mathcal{E}) \equiv \frac{P(\mathcal{E})\mathcal{D}(\mathcal{E})}{\mathcal{R}_{\text{lc}}(\mathcal{E})}. \quad (23)$$

where $q_{\text{lc}} \gtrsim 1$ defines the full-loss-cone regime. Since the limiting value of \mathcal{D} as $\mathcal{R} \rightarrow 0$ may not be well defined it is more useful to define \mathcal{D} as

$$\mathcal{D}(\mathcal{E}) \equiv \left. \frac{\langle (\Delta \mathcal{R})^2 \rangle_t}{2\mathcal{R}} \right|_{\mathcal{R}=\mathcal{R}_{\text{lc}}} = \frac{D_{\mathcal{R}\mathcal{R}}(\mathcal{E}, \mathcal{R}_{\text{lc}})}{\mathcal{R}_{\text{lc}}}. \quad (24)$$

3. DIFFUSION COEFFICIENTS

3.1. Cohn-Kulsrud diffusion coefficients

Orbit-averaged diffusion coefficients were derived by Cohn & Kulsrud (1978) for stars moving in a Kepler potential. Their derivation was based on the theory of random gravitational encounters as developed by Chandrasekhar, Hénon, Spitzer and others. Cohn & Kulsrud wrote their orbit-averaged diffusion coefficients as

$$\begin{aligned} \langle \Delta \mathcal{E} \rangle_t &= -F_0 + F_1, & \langle (\Delta \mathcal{E})^2 \rangle_t &= \frac{4}{3} \mathcal{E} F_0 + \frac{4}{3} \mathcal{E} F_4, & \langle \Delta \mathcal{E} \Delta \mathcal{R} \rangle_t &= \frac{4\mathcal{R}}{3} F_4 - \frac{4\mathcal{R}}{3} F_5, \\ \langle \Delta \mathcal{R} \rangle_t &= \frac{5}{3\mathcal{E}} (1 - 2\mathcal{R}) F_0 + \frac{\mathcal{R}}{\mathcal{E}} F_1 - \frac{5\mathcal{R}}{2\mathcal{E}} F_2 + \frac{4}{\mathcal{E}} F_3 - \frac{4\mathcal{R}}{3\mathcal{E}} F_5 + \frac{\mathcal{R}}{2\mathcal{E}} F_6 - \frac{4}{3\mathcal{E}} F_7, \\ \langle (\Delta \mathcal{R})^2 \rangle_t &= \frac{10\mathcal{R}}{3\mathcal{E}} (1 - \mathcal{R}) F_0 - 2\frac{\mathcal{R}^2}{\mathcal{E}} F_2 + 8\frac{\mathcal{R}}{\mathcal{E}} F_3 + \frac{4\mathcal{R}^2}{3\mathcal{E}} F_4 - \frac{8\mathcal{R}^2}{3\mathcal{E}} F_5 + 2\frac{\mathcal{R}^2}{\mathcal{E}} F_6 - \frac{8\mathcal{R}}{3\mathcal{E}} F_7 \end{aligned} \quad (25)$$

where the functions F_i , $i = 0 \dots 7$ are expressed as integrals depending on f . We follow those authors and assume that the F_i depend only on the angular-momentum average of f , or

$$\bar{f}(\mathcal{E}, t) \equiv \int_0^1 f(\mathcal{E}, \mathcal{R}, t) d\mathcal{R}. \quad (26)$$

With this simplification, Cohn & Kulsrud show that the F_i are

$$F_0(\mathcal{E}) = 4\pi\Gamma \int_0^{\mathcal{E}} \bar{f}(\mathcal{E}') d\mathcal{E}', \quad (27a)$$

$$F_i(\mathcal{E}, \mathcal{R}) = 4\pi\Gamma \int_{\mathcal{E}}^{\mathcal{E}/x_-} \bar{f}(\mathcal{E}') C_i \left(\frac{\mathcal{E}'}{\mathcal{E}}, \mathcal{R} \right) d\mathcal{E}', \quad (27b)$$

where $\Gamma \equiv 4\pi G^2 m_\star^2 \ln \Lambda$, $\ln \Lambda$ is the Coulomb logarithm, and $x_{\pm} \equiv \frac{1}{2} [1 \pm (1 - \mathcal{R})^{1/2}]$. The functions C_i ($s = \mathcal{E}'/\mathcal{E}, \mathcal{R}$) have the forms

$$C_i = \frac{2}{\pi} \int dx Q^{-1/2} \frac{x^l (1 - sx)^{m/2}}{(1 - x)^{n/2}}$$

with (l, m, n) integers and $Q \equiv (x_+ - x)(x - x_-)$. Appendix A gives explicit expressions for the C_i and describes how they were computed numerically.

Henceforth the diffusion coefficients (25) will be referred to as the Cohn-Kulsrud (CK) diffusion coefficients and given the subscript ‘‘CK.’’ The subscript t , for orbit-averaging, is understood in everything that follows and will be omitted henceforth.

The quantity $\mathcal{D}(\mathcal{E}) \equiv [\langle (\Delta \mathcal{R})^2 \rangle_t / (2\mathcal{R})]_{\mathcal{R}=\mathcal{R}_{\text{lc}}}$ defined in equation (24), which is effectively an orbit-averaged, angular momentum relaxation time, can be written in terms of the F_i as

$$\mathcal{D}(\mathcal{E}) = \frac{1}{3\mathcal{E}} [5F_0(\mathcal{E}) + 12F_3(\mathcal{E}, \mathcal{R}_{\text{lc}}) - 4F_7(\mathcal{E}, \mathcal{R}_{\text{lc}})] \quad (28)$$

and the quantity q_{lc} defined in equation (23) is

$$q_{lc}(\mathcal{E}) = \frac{\pi}{3\sqrt{2}} \frac{GM_{\bullet}}{\mathcal{E}^{5/2}} \frac{1}{\mathcal{R}_{lc}(\mathcal{E})} [5F_0(\mathcal{E}) + 12F_3(\mathcal{E}, \mathcal{R}_{lc}) - 4F_7(\mathcal{E}, \mathcal{R}_{lc})]. \quad (29)$$

3.2. Resonant relaxation

The theory of random gravitational encounters that is the basis for the Cohn-Kulsrud diffusion coefficients fails to adequately describe the evolution of orbits sufficiently near to a SBH, where motion is close to Keplerian and where orbits maintain their orientations for many periods (Rauch & Tremaine 1996). In this regime, it is common to assume that random gravitational encounters are still active at changing orbital E and L , according to the diffusion coefficients defined above, but that torques due to the nearly-fixed Keplerian orbits are also effective at changing L , sometimes on time scales much shorter than the relaxation time defined in terms of random encounters (Hopman & Alexander 2006; Eilon et al. 2009).

We make the same assumptions here, and write the diffusion coefficients that appear in the Fokker-Planck equation as (orbit-averaging understood)

$$\begin{aligned} \langle \Delta \mathcal{E} \rangle &= \langle \Delta \mathcal{E} \rangle_{\text{CK}}, & \langle (\Delta \mathcal{E})^2 \rangle &= \langle (\Delta \mathcal{E})^2 \rangle_{\text{CK}}, & \langle \Delta \mathcal{E} \Delta \mathcal{R} \rangle &= \langle \Delta \mathcal{E} \Delta \mathcal{R} \rangle_{\text{CK}}, \\ \langle \Delta \mathcal{R} \rangle &= \langle \Delta \mathcal{R} \rangle_{\text{CK}} + \langle \Delta \mathcal{R} \rangle_{\text{RR}}, & \langle (\Delta \mathcal{R})^2 \rangle &= \langle (\Delta \mathcal{R})^2 \rangle_{\text{CK}} + \langle (\Delta \mathcal{R})^2 \rangle_{\text{RR}}. \end{aligned} \quad (30)$$

It is understood that the resonant diffusion coefficients describe changes in L in the “incoherent” (as opposed to the “coherent”) regime, i.e., on time scales long compared with the coherence time (defined below).

No very complete theory of incoherent resonant relaxation exists. While the approximate dependence of the diffusion rate on energy (i.e. distance from the SBH) is not difficult to derive, until recently, little was known about the angular-momentum dependence of the first- and second-order L -diffusion coefficients. We base what follows on the numerical treatment of Hamers, Portegies Zwart & Merritt (2014), who used an algorithm called TPI (“test-particle integrator”) to infer values of the angular momentum diffusion coefficients for test stars orbiting in nuclei with $n(r) \propto r^{-2}$ and r^{-1} .

Those authors expressed the diffusion coefficients in terms of the angular momentum variable

$$\ell \equiv \frac{L}{L_c(E)} = \mathcal{R}^{1/2} = \sqrt{1 - e^2}. \quad (31)$$

A straightforward transformation yields the relations between diffusion coefficients in ℓ and in \mathcal{R} :

$$\langle \Delta \mathcal{R} \rangle = 2\ell \langle \Delta \ell \rangle + \langle (\Delta \ell)^2 \rangle, \quad \langle (\Delta \mathcal{R})^2 \rangle = 4\ell^2 \langle (\Delta \ell)^2 \rangle \quad (32)$$

or

$$\langle \Delta \ell \rangle = \frac{1}{2\sqrt{\mathcal{R}}} \langle \Delta \mathcal{R} \rangle - \frac{1}{8\mathcal{R}^{3/2}} \langle (\Delta \mathcal{R})^2 \rangle, \quad \langle (\Delta \ell)^2 \rangle = \frac{1}{4\mathcal{R}} \langle (\Delta \mathcal{R})^2 \rangle. \quad (33)$$

Hamers et al. (2014) proposed the following forms for the the first- and second-order diffusion coefficients:

$$\langle \Delta \ell \rangle_{\text{RR}} = C_1 A(\mathcal{E}) g(\ell) \quad \langle (\Delta \ell)^2 \rangle_{\text{RR}} = C_2 A(\mathcal{E}) h(\ell) \quad (34a)$$

$$A(a) = \alpha_s^2 \left[\frac{M_{\star}(a)}{M_{\bullet}} \right]^2 \frac{1}{N(a)} \frac{t_{\text{coh}}(a)}{P(a)^2} \quad (34b)$$

$$g(\ell) = \frac{1}{\ell} \left(1 - \frac{\ell^2}{\ell_c^2} \right), \quad h(\ell) = 1 - \ell^2. \quad (34c)$$

In these expressions, a is related to \mathcal{E} via equation (5). The value of α_s was determined numerically to be ~ 1.6 , and ℓ_c was estimated to be ~ 0.7 , weakly dependent on a . Hamers et al. suggested $C_1 \approx C_2 \approx 1$. The quantity $t_{\text{coh}}(a)$ in equations (34) is the “coherence time,” defined as the typical time, for stars of semimajor axis a , to precess by an angle π . Hamers et al. assumed¹

$$t_{\text{coh}}^{-1} \equiv t_{\text{coh},\text{M}}^{-1} + t_{\text{coh},\text{S}}^{-1} \quad (35)$$

where

$$t_{\text{coh},\text{M}}(a) = \frac{M_{\bullet}}{N(a)m_{\star}} P(a), \quad t_{\text{coh},\text{S}}(a) = \frac{1}{12} \frac{a}{r_g} P(a). \quad (36)$$

The latter are averages over eccentricity of the mass- and Schwarzschild apsidal precession times, respectively, assuming a “thermal” eccentricity distribution, $N(e; a)de \propto ede$ (Merritt 2013, §5.6.1.1). The Schwarzschild coherence time is

¹ Some authors, e.g. Hopman & Alexander (2006) and Madigan et al. (2011), define the coherence time in terms of a *difference* between the two precession rates, implying an infinite coherence time at some radius. The reason why this is incorrect is discussed in Merritt (2013), §5.6.1.

independent of the mass distribution and is given by

$$t_{\text{coh,S}}(a) = \frac{\pi}{6} \frac{c^2 a^{5/2}}{(GM_\bullet)^{3/2}} \approx 5.1 \times 10^3 \left(\frac{M_\bullet}{10^6 M_\odot} \right)^{-3/2} \left(\frac{a}{10^{-3} \text{pc}} \right)^{5/2} \text{ yr.} \quad (37)$$

The mass coherence time depends on the stellar distribution. These two coherence times are equal when

$$aN(a) = 12 \frac{M_\bullet}{m_\star} r_g \quad (38)$$

In the approximate theory that motivated the expression (34) for $A(a)$, the quantity $N(a)$ could mean either “number of stars with instantaneous radii less than a ” or “number of stars with semimajor axes less than a ”. In fact, these two functions are quite similar, at least in nuclei with steeply-rising density near the SBH (Appendix B). In his numerical experiments, A. Hamers (private communication) was not able to determine which definition of $N(a)$ provided the better fit to the data. In what follows, we adopt the first definition, which is simpler to implement in the code:

$$N(a) = 4\pi \int_0^a n(r) r^2 dr \quad (39)$$

and $M_\star(a) = m_\star N(a)$.

The a -dependence of the diffusion coefficients in equations (34) is based on theoretical arguments, but the ℓ -dependence is essentially ad hoc. While the diffusion coefficients derived numerically by Hamers et al. were consistent with the ℓ dependence of equations (34), the functional forms themselves were not strongly constrained. We now consider those functional forms in more detail.

The variables ℓ or \mathcal{R} are bounded, and therefore the flux in \mathcal{R} :

$$\phi_{\mathcal{R}} = -D_{\mathcal{R}} f - D_{\mathcal{R}\mathcal{R}} \frac{\partial f}{\partial \mathcal{R}} \quad (40)$$

must go to zero as $\mathcal{R} \rightarrow 0$ or $\mathcal{R} \rightarrow 1$. Furthermore this must be true for any $f(\mathcal{R})$ in equation (40). Hence we require

$$D_{\mathcal{R}} \rightarrow 0, \quad D_{\mathcal{R}\mathcal{R}} \rightarrow 0 \quad (41)$$

as $\mathcal{R} \rightarrow \{0, 1\}$. According to equations (18) and (32),

$$D_{\mathcal{R}} = -\langle \Delta \mathcal{R} \rangle + \frac{1}{2} \frac{\partial}{\partial \mathcal{R}} \langle (\Delta \mathcal{R})^2 \rangle = -2\ell \langle \Delta \ell \rangle + \langle (\Delta \ell)^2 \rangle + \ell \frac{\partial}{\partial \ell} \langle (\Delta \ell)^2 \rangle \quad (42a)$$

$$D_{\mathcal{R}\mathcal{R}} = \frac{1}{2} \langle (\Delta \mathcal{R})^2 \rangle = 2\ell^2 \langle (\Delta \ell)^2 \rangle. \quad (42b)$$

Equations (41) - (42) imply

$$\langle \Delta \mathcal{R} \rangle \rightarrow \frac{1}{2} \frac{\partial}{\partial \mathcal{R}} \langle (\Delta \mathcal{R})^2 \rangle, \quad \langle (\Delta \mathcal{R})^2 \rangle \rightarrow 0 \quad (43a)$$

$$\ell \langle \Delta \ell \rangle \rightarrow \frac{1}{2} \frac{\partial}{\partial \ell} [\ell \langle (\Delta \ell)^2 \rangle], \quad \ell^2 \langle (\Delta \ell)^2 \rangle \rightarrow 0 \quad (43b)$$

as $\{\mathcal{R}, \ell\} \rightarrow 0$ or 1 .

The expression for $\langle (\Delta \ell)^2 \rangle$ in equation (34) satisfies these conditions.

In the case of the first-order coefficient for ℓ , the condition (43b) becomes

$$C_1 \ell g(\ell) = \frac{C_2}{2} \frac{\partial}{\partial \ell} [\ell h(\ell)], \quad \ell \rightarrow \{0, 1\} \quad (44)$$

i.e.

$$C_1 \left(1 - \frac{\ell^2}{\ell_c^2} \right) = \frac{C_2}{2} (1 - 3\ell^2), \quad \ell \rightarrow \{0, 1\}. \quad (45)$$

Applying this respectively at $\ell = \{0, 1\}$ yields

$$C_1 = \frac{C_2}{2} \quad (\ell = 0), \quad (46a)$$

$$C_1 (1 - \ell_c^2) = C_2 \ell_c^2 \quad (\ell = 1) \quad (46b)$$

and therefore

$$\ell_c = \frac{1}{\sqrt{3}} \approx 0.577 \quad (C_2 = 2C_1). \quad (47)$$

Interestingly, the first-order flux coefficient implied by these functional forms:

$$\begin{aligned} D_{\mathcal{R}}(\ell) &= A(E) \left[-2C_1 \left(1 - \frac{\ell^2}{\ell_c^2} \right) + C_2 (1 - \ell^2) + \ell C_2 (-2\ell) \right] \\ &= A(E) [(C_2 - 2C_1) \ell_c^2 + (2C_1 - 3C_2 \ell_c^2) \ell^2] \end{aligned} \quad (48)$$

is identically zero if we choose $\{C_2 = 2C_1, \ell_c^2 = 1/3\}$. Hence, imposing $D_{\mathcal{R}} = 0$ at the boundaries implies $D_{\mathcal{R}} = 0$ everywhere – though not necessarily zero *flux* everywhere.

Based on their numerical experiments, Hamers, Portegies Zwart & Merritt (2014) suggested a different choice of parameters: $C_1 = C_2$ and $\ell_c \approx 0.7$. Indeed, setting $C_1 = C_2$ in equation (46b) yields

$$\ell_c = \frac{1}{\sqrt{2}} \approx 0.707 \quad (C_2 = C_1). \quad (49)$$

The implied flux coefficient is

$$D_{\mathcal{R}} = -\frac{C_1}{2} (1 - \ell^2), \quad (50)$$

zero at $\ell = 1$ but not at $\ell = 0$.

In face of these issues, we returned to the numerical results of Hamers et al. and considered more general functional forms for the diffusion coefficients.

The \mathcal{R} -diffusion coefficients implied by equations (34) have the forms

$$\langle \Delta \mathcal{R} \rangle = A(E) [(2C_1 + C_2) - (C_2 + 2C_1/\ell_c^2) \mathcal{R}], \quad (51a)$$

$$\langle (\Delta \mathcal{R})^2 \rangle = A(E) \times 4C_2 \mathcal{R} (1 - \mathcal{R}), \quad (51b)$$

linear in the case of the first-order coefficient and quadratic in the case of the second-order coefficient. Consider the more general functional forms

$$\langle \Delta \mathcal{R} \rangle = A(E) (a + b\mathcal{R} + c\mathcal{R}^2), \quad (52a)$$

$$\langle (\Delta \mathcal{R})^2 \rangle = A(E) (d + e\mathcal{R} + f\mathcal{R}^2) \quad (52b)$$

which adds an extra parameter, for a total of six. We now require that these parameters be chosen so as to satisfy all the following conditions:

1. $\langle (\Delta \mathcal{R})^2 \rangle \geq 0$
2. $\langle (\Delta \mathcal{R})^2 \rangle = 0$ for $\mathcal{R} = \{0, 1\}$
3. $\langle \Delta \mathcal{R} \rangle = \frac{1}{2} \frac{\partial}{\partial \mathcal{R}} \langle (\Delta \mathcal{R})^2 \rangle$ for $\mathcal{R} = \{0, 1\}$

It is easy to show that these conditions leave only two independent parameters, allowing the diffusion coefficients (52) to be written as

$$\langle \Delta \mathcal{R} \rangle = A(E) \times C [1 - \eta \mathcal{R} + (\eta - 2) \mathcal{R}^2], \quad (53a)$$

$$\langle (\Delta \mathcal{R})^2 \rangle = A(E) \times 2C \times \mathcal{R} (1 - \mathcal{R}). \quad (53b)$$

The parameter C is a normalization; based on comparison with equation (51), we expect $C = 2C_1 + C_2 \approx 2$. The parameter η can have any value; it determines the value of \mathcal{R} at which $\langle \Delta \mathcal{R} \rangle = 0$, i.e. the value of $x \equiv \mathcal{R}_0$ that solves

$$(\eta - 2)x^2 - \eta x + 1 = 0 \quad (54)$$

(there is only one root in the range $x \in [0, 1]$). $\eta = \infty$ corresponds to $\mathcal{R}_0 = 0$ and $\eta = -\infty$ to $\mathcal{R}_0 = 1$.

A. Hamers kindly provided data files with the numerically-determined diffusion coefficients, as presented in the Hamers et al. 2014 paper. The best-fitting values of $\{C, \eta\}$ were determined from these data, at each semimajor axis bin, as follows:

1. Given the numerically-computed diffusion coefficients in ℓ , the 1st- and 2nd-order diffusion coefficients in \mathcal{R} were computed at each of the data points \mathcal{R}_i using equations (32). To simplify the notation, we call these $D_1(\mathcal{R}_i)$ and $D_2(\mathcal{R}_i)$ respectively.
2. Data were excluded if they lay outside the range $\ell_1 \leq \ell \leq \ell_2$, with $\ell_2 = 0.95$ and ℓ_1 equal to 1.1 times the predicted location of the ‘‘Schwarzschild barrier’’ (as defined below).
3. The quantity

$$\sum_{\text{data}} \{D_1(\mathcal{R}_i) - C [1 - \eta \mathcal{R}_i + (\eta - 2) \mathcal{R}_i^2]\}^2 + [D_2(\mathcal{R}_i) - 2C \mathcal{R}_i (1 - \mathcal{R}_i)]^2$$

was minimized on a grid in $\{C, \eta\}$.

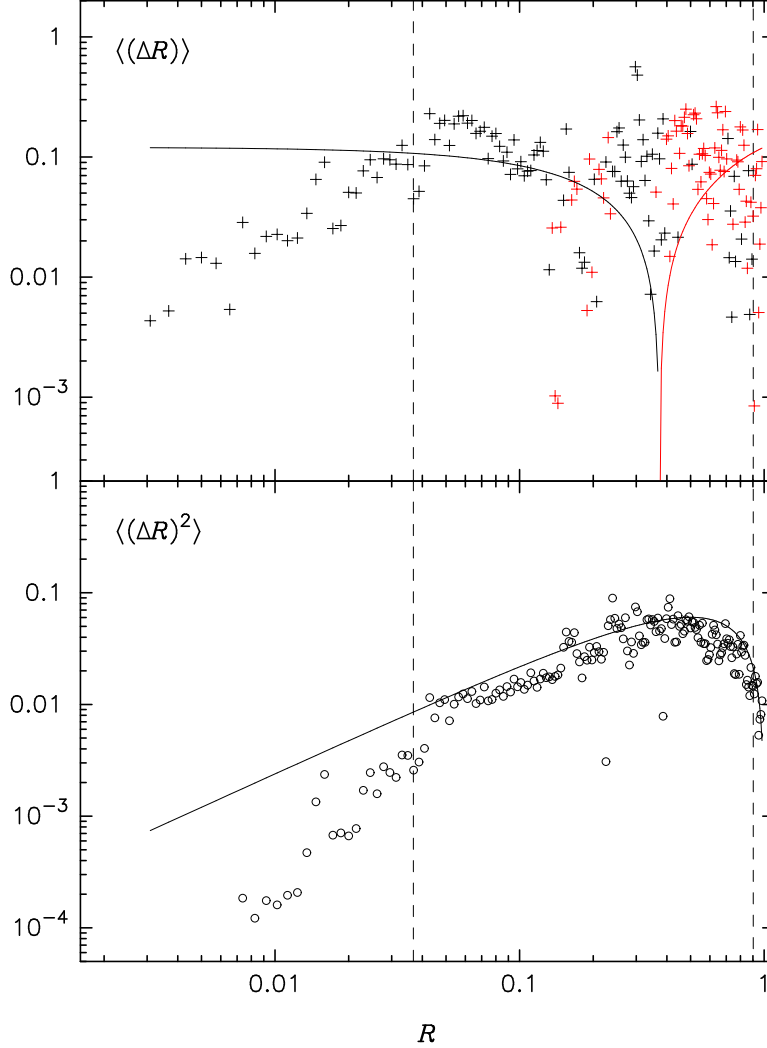


FIG. 1.— Fits to the diffusion coefficient data from Hamers, Portegies Zwart & Merritt (2014) for the radial bin $\langle a \rangle = 19.9$ mpc. In the upper panel, red symbols are $-\langle \Delta \mathcal{R} \rangle$. Dashed vertical lines delineate the region in which data were fit to the analytic forms (53); the latter are shown as the solid curves.

Figure 1 shows the fits to the data in the bin $\langle a \rangle = 19.9$ mpc.

Figure 2 shows \mathcal{R}_0 as a function of a . There is much scatter, but the mean value is close to $\mathcal{R}_0 = 0.5$ ($\eta = 2$) and there is no obvious trend with a .

Based on these results, the following functional forms were adopted:

$$\langle \Delta \mathcal{R} \rangle_{\text{RR}} = 2A(E) (1 - 2\mathcal{R}), \quad (55a)$$

$$\langle (\Delta \mathcal{R})^2 \rangle_{\text{RR}} = 4A(E) \mathcal{R} (1 - \mathcal{R}). \quad (55b)$$

Note that the \mathcal{R}^2 term in $\langle \Delta \mathcal{R} \rangle$ vanishes for the adopted value of $\eta = 2$. The corresponding diffusion coefficients in ℓ are

$$\langle \Delta \ell \rangle_{\text{RR}} = A(E) \frac{(1 - 3\ell^2)}{2\ell}, \quad (56a)$$

$$\langle (\Delta \ell)^2 \rangle_{\text{RR}} = A(E) (1 - \ell^2) \quad (56b)$$

implying $\langle \Delta \ell \rangle = 0$ at $\ell = 1/\sqrt{3} \approx 0.58$, consistent with Figure 2b.

In what follows, equations (55) are assumed to define the RR diffusion coefficients in equations (30).

Given these choices, and setting changes in E to zero, the flux coefficients have the simple forms

$$D_{\mathcal{R}}(\mathcal{R}) = 0, \quad D_{\mathcal{R}\mathcal{R}}(\mathcal{R}) = 2A(E)\mathcal{R}(1 - \mathcal{R}) \quad (57)$$

and the \mathcal{R} - directed flux is

$$F_{\mathcal{R}} = -2A(E)\mathcal{R}(1 - \mathcal{R}) \frac{\partial f}{\partial \mathcal{R}} \quad (58)$$

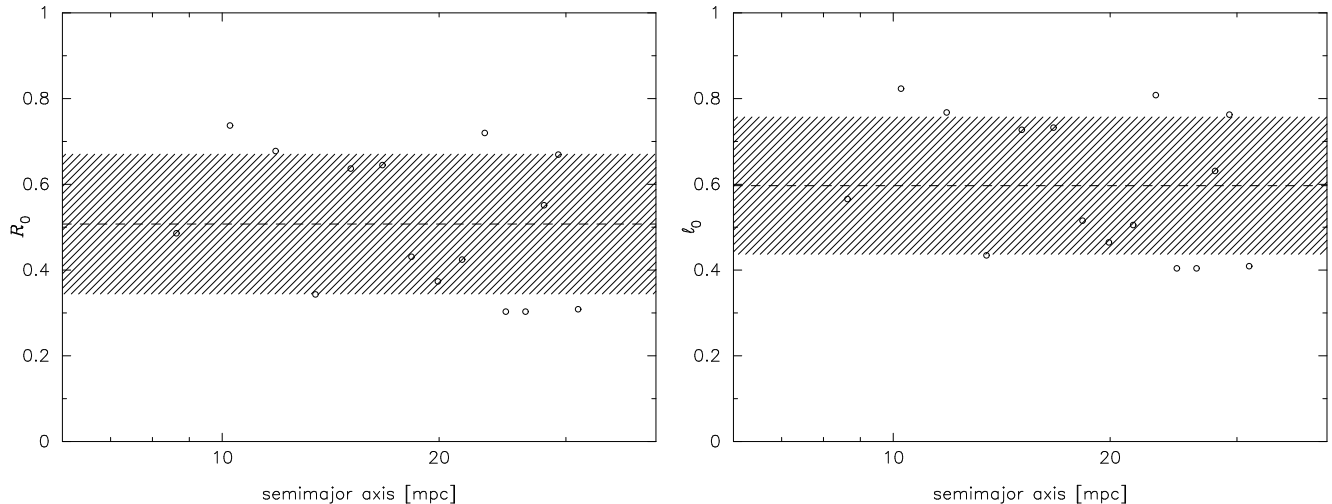


FIG. 2.— The parameter η in the fits, shown here in terms of the value of \mathcal{R} where the first-order diffusion coefficient in \mathcal{R} is zero (left), and the value of ℓ where the first-order diffusion coefficient in ℓ is zero (right). Dashed horizontal lines are unweighted means of the plotted points.

which has the correct behavior at $\mathcal{R} = \{0, 1\}$. The zero-flux solution is therefore $f(\mathcal{R}) = \text{const}$, as in the NR case. The constant-flux solution, with boundary condition $f = 0$ at $\mathcal{R} = \mathcal{R}_{\text{lc}}$, is

$$f(\mathcal{R}) = f_0 \log \left[\frac{1 - \mathcal{R}_{\text{lc}}}{1 - \mathcal{R}} \frac{\mathcal{R}}{\mathcal{R}_{\text{lc}}} \right] \quad (59)$$

and the flux is $-2A(E)f_0$. Since

$$f(E) \approx \bar{f} \equiv \int f(\mathcal{R}) d\mathcal{R} = -f_0 \log \mathcal{R}_{\text{lc}}, \quad (60)$$

we can write

$$f_0 \approx \frac{f(E)}{\log(1/\mathcal{R}_{\text{lc}})} \quad (61)$$

yielding for the flux

$$\phi_{\mathcal{R}} \approx -\frac{2A(E)f(E)}{\log(1/\mathcal{R}_{\text{lc}})}. \quad (62)$$

We expect these expressions to be only approximate since in reality, the steady-state solutions will have nonzero fluxes in the $E-$ direction.

We also give here the expression for \mathcal{D} , equation (24), in the RR regime:

$$\mathcal{D} = \left[\frac{\langle (\Delta \mathcal{R})^2 \rangle_t}{2\mathcal{R}} \right]_{\mathcal{R}_{\text{lc}}} = 2\alpha_s^2 \left(\frac{M_\star}{M_\bullet} \right)^2 \frac{1}{N} \frac{t_{\text{coh}}}{P^2}. \quad (63)$$

Using the approximate expression for \mathcal{R}_{lc} in equation (11) (corresponding to the capture radius for a compact object), the quantity q_{lc} defined in equation (23) becomes

$$q_{\text{lc}}(a) \approx \frac{\alpha_s^2}{8} \left(\frac{m_\star}{M_\bullet} \right)^2 N \frac{t_{\text{coh}}}{P} \frac{a}{r_g}. \quad (64)$$

Assuming respectively that $t_{\text{coh}} = \{t_{\text{coh},\text{M}}, t_{\text{coh},\text{S}}\}$ yields

$$q_{\text{lc},\text{M}} = \frac{\alpha_s^2}{8} \frac{m_\star}{M_\bullet} \frac{a}{r_g}, \quad q_{\text{lc},\text{S}} = \frac{\alpha_s^2}{96} \left(\frac{m_\star}{M_\bullet} \right)^2 N(a) \left(\frac{a}{r_g} \right)^2. \quad (65)$$

Note the interesting result that $q_{\text{lc},\text{M}}$ does not depend on the mass distribution, while $q_{\text{lc},\text{S}}$ does. The former is

$$q_{\text{lc},\text{M}} \approx 0.07 \left(\frac{M_\bullet/m_\star}{10^5} \right)^{-1} \left(\frac{M_\bullet}{10^6 M_\odot} \right)^{-1} \frac{a}{\text{mpc}}. \quad (66)$$

3.3. Anomalous relaxation

The diffusion coefficients defined in the previous section are affected by general relativity (GR) to the extent that GR determines the coherence time; the latter defined as a *typical* precession time of all stars at a given radius. Another GR-related phenomenon is the ‘‘Schwarzschild barrier’’ (SB), the tendency of *single*, very eccentric orbits not to diffuse in L below some definite value at each a . The SB was first observed in N -body simulations (Merritt et al. 2011), as a locus in the $\log a$ vs. $\log(1 - e)$ plane where the orbital trajectories ‘‘bounced’’ in the course of their RR-driven random walks in L . The same study revealed that orbits experiencing the ‘‘bounce’’ were of such high eccentricity that their GR precession times were short compared with those of typical (i.e., higher- L) stars at the same a . Hamers, Portegies Zwart & Merritt (2014) coined the term ‘‘anomalous relaxation’’ to describe the behavior of orbits in this high-eccentricity regime.

Two analytic expressions have been proposed for the location of the SB. The first is based on a comparison of the GR precession time with the time for the \sqrt{N} torques to change L (Merritt et al. 2011):

$$\mathcal{R}_{\text{SB}}^{(i)}(a) \approx \left(\frac{r_g}{a}\right)^2 \left[\frac{M_\bullet}{M_\star(a)}\right]^2 N(a). \quad (67)$$

The second (Hamers, Portegies Zwart & Merritt 2014) compares the GR precession time with the coherence time:

$$\mathcal{R}_{\text{SB}}^{(ii)}(a) \approx 4 \frac{r_g t_{\text{coh}}(a)}{a P(a)}. \quad (68)$$

In spite of their disparate functional forms, the two expressions yield numerically similar relations for $\mathcal{R}_{\text{SB}}(a)$ in a wide range of nuclear models. However the former relation appears to more accurately reproduce the barrier location in numerical studies to date (Merritt et al. 2011; Hamers, Portegies Zwart & Merritt 2014).

Appendix C derives expressions for the diffusion coefficients in this regime, based on a simple Hamiltonian model (Merritt et al. 2011):

$$\langle \Delta \ell \rangle \approx \frac{2\ell^3}{\tau}, \quad \langle (\Delta \ell)^2 \rangle \approx \frac{\ell^4}{\tau} \quad (69)$$

where $\tau(a) \equiv t_{\text{coh}}(a)/(A_{\sqrt{N}})^2$ and

$$A_{\sqrt{N}} \equiv \frac{1}{2\sqrt{N(a)}} \frac{M_\star(a)}{M_\bullet} \frac{a}{r_g}. \quad (70)$$

Hamers, Portegies Zwart & Merritt (2014) verified the ℓ -dependence predicted by equation (69) via numerical experiments. Expressed in terms of \mathcal{R} via equations (32), the diffusion coefficients become

$$\langle \Delta \mathcal{R} \rangle_{\text{AR}} = \frac{5}{\tau} \mathcal{R}^2, \quad \langle (\Delta \mathcal{R})^2 \rangle_{\text{AR}} = \frac{4}{\tau} \mathcal{R}^3. \quad (71)$$

Equations (71) replace equations (55) when $\mathcal{R} \leq \mathcal{R}_{\text{SB}}$. We note that the values of the numerical coefficients in these expressions have not been well determined by the numerical experiments to date, and the simple model in Appendix C is not likely to be valid when \mathcal{R} is so small that the GR precession time is much shorter than the coherence time. Additional N -body experiments are needed to elucidate the functional forms of the anomalous diffusion coefficients. Solutions to the Fokker-Planck equation containing these diffusion coefficients will be postponed to Paper III in this series (Merritt 2015b).

3.4. Gravitational radiation

First-order diffusion coefficients in \mathcal{E} and \mathcal{R} also exist that describe changes due to emission of gravitational waves. At the lowest (2.5 PN) order, the orbit-averaged rates of change of a and e are:

$$\langle \Delta a \rangle = -\frac{64}{5} \frac{G^3 M_\bullet^2 m_\star}{c^5 a^3 (1 - e^2)^{7/2}} \left(1 + \frac{73}{24} e^2 + \frac{37}{96} e^4\right), \quad (72a)$$

$$\langle \Delta e \rangle = -\frac{304}{15} \frac{G^3 M_\bullet^2 m_\star e}{c^5 a^4 (1 - e^2)^{5/2}} \left(1 + \frac{121}{304} e^2\right) \quad (72b)$$

(equations 4.234 from Merritt (2013) after replacing $m_1 m$ in those expressions by M_\bullet^2). Expressed in terms of $\mathcal{E} = GM_\bullet/(2a)$ and $\mathcal{R} = 1 - e^2$,

$$\langle \Delta \mathcal{E} \rangle = -\frac{2\mathcal{E}^2}{GM_\bullet} \langle \Delta a \rangle = \frac{2720}{3} \frac{m_\star}{M_\bullet} \frac{1}{GM_\bullet c^5} \frac{\mathcal{E}^5}{\mathcal{R}^{7/2}} \left(1 - \frac{366}{425} \mathcal{R} + \frac{37}{425} \mathcal{R}^2\right), \quad (73a)$$

$$\langle \Delta \mathcal{R} \rangle = -2\sqrt{1 - \mathcal{R}} \langle \Delta e \rangle = \frac{2720}{3} \frac{m_\star}{M_\bullet} \frac{1}{GM_\bullet c^5} \frac{\mathcal{E}^4}{\mathcal{R}^{5/2}} \left(1 - \frac{546}{425} \mathcal{R} + \frac{121}{425} \mathcal{R}^2\right). \quad (73b)$$

4. NUMERICAL ALGORITHM

4.1. Choice of grid and units

Solutions are obtained on a $(N_x \times N_z)$ grid in (X, Z) , where

$$X \equiv \ln R = \ln \left[\frac{L}{L_c(\mathcal{E})} \right]^2 = \ln(1 - e^2), \quad (74a)$$

$$Z \equiv \ln(1 + \beta \mathcal{E}^*) = \ln(1 + \beta \mathcal{E}/c^2) \quad (74b)$$

(Figure 3). Typically $N_x = N_z = 64$. Here and below, starred variables are dimensionless, based on code units which are

$$G = M_\bullet = c = 1. \quad (75)$$

Thus $\mathcal{E} = c^2 \mathcal{E}^*$ and $L = (GM_\bullet/c)L^*$. The angular momentum of a circular orbit, $L_c = \sqrt{GM_\bullet/(2\mathcal{E})}$, becomes in dimensionless units $L_c^* = 1/(2\mathcal{E}^*)$. The squared angular momentum of an orbit with periapsis at $r = 8r_g$ is

$$R_{lc}(\mathcal{E}^*) = 32\mathcal{E}^*(1 - 8\mathcal{E}^*), \quad \mathcal{E}^* \leq \frac{1}{16}. \quad (76)$$

In the code, all diffusion coefficients are divided by the factor $\Gamma \equiv 4\pi G^2 m_\star^2 \ln \Lambda$. The dimensional factor f_0 multiplying f^* is taken to be

$$f_0 = \left(\frac{r_m}{r_g} \right)^\gamma \left(\frac{M_\bullet}{m_\star} \right) \frac{1}{c^3 r_m^3}. \quad (77)$$

These two choices determine the unit of time as $(\Gamma f_0)^{-1}$ or

$$[t] \equiv t_0 = \frac{1}{4\pi \ln \Lambda} \left(\frac{M_\bullet}{m_\star} \right) \left(\frac{r_m}{r_g} \right)^{2-\gamma} \left(\frac{r_m}{c} \right) = 1.7 \times 10^{-4} \text{yr} \left(\frac{\ln \Lambda}{15} \right)^{-1} \left(\frac{M_\bullet/m_\star}{10^5} \right) \left(\frac{r_m}{r_g} \right)^{3-\gamma}. \quad (78)$$

In these expressions, r_m and γ are free parameters, but they have a simple physical interpretation in the case of a cluster with a power-law density:

$$n(r) = n_0 \left(\frac{r}{r_m} \right)^{-\gamma}, \quad n_0 = \frac{3-\gamma}{2\pi} \frac{M_\bullet}{m_\star} \frac{1}{r_m^3} \quad (79)$$

for which r_m is the radius containing a mass in stars equal to $2M_\bullet$. The isotropic f corresponding to the density (79) is

$$f(\mathcal{E}) = f_0 f^*(\mathcal{E}^*) = f_0 C(\gamma) \mathcal{E}^{\star \gamma - 3/2}, \quad C(\gamma) = \frac{3-\gamma}{8} \sqrt{\frac{2}{\pi^5}} \frac{\Gamma(\gamma+1)}{\Gamma(\gamma-1/2)}. \quad (80)$$

Initial conditions were typically chosen to be equations (79) – (80) or some modification, e.g., f might be set initially to zero inside the loss cone, as described in more detail below. When the initial f was constructed in this way, r_m and γ retain their meaning as the parameters describing the unmodified power-law model.

The initial density normalization (stars per unit volume) is fixed by the choice of $r_m^* = r_m/r_g$. At any later time, the dimensionless number density:

$$n^*(r^*) = \int f^* d^3 v^* \quad (81)$$

is related to the true number density by

$$n(r) = \int f d^3 v = c^3 f_0 \int f^* d^3 v^* = \frac{1}{r_g^3} \left(\frac{r_m}{r_g} \right)^{\gamma-3} \frac{M_\bullet}{m_\star} n^*(r^*). \quad (82)$$

Similarly the number of stars within r is

$$N(< r) = \left(\frac{r_m}{r_g} \right)^{\gamma-3} \left(\frac{M_\bullet}{m_\star} \right) N^*(< r^*) \quad (83)$$

where $N^*(r^*) = 4\pi \int_0^{r^*} n^*(r^*) r^{*2} dr^*$. These expressions are used when evaluating the diffusion coefficients in the RR and AR regimes. Combining equations (78) and (83), the rate of loss of stars from within a sphere of radius r is given in terms of dimensionless quantities as

$$\frac{dN(< r)}{dt} = 4\pi \ln \Lambda \frac{c}{r_g} \left(\frac{r_m}{r_g} \right)^{2(\gamma-3)} \frac{dN^*(< r^*)}{dt^*}. \quad (84)$$

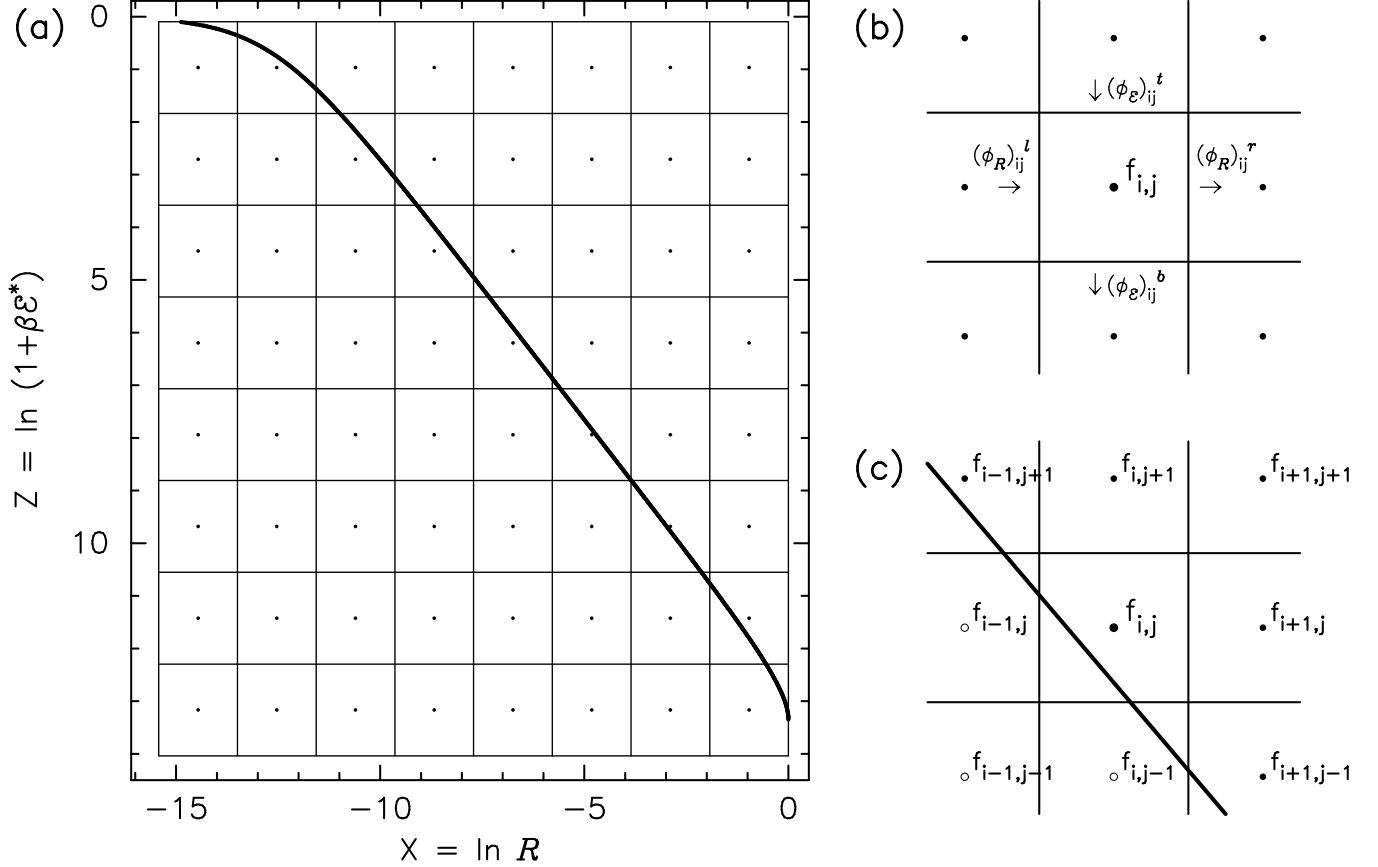


FIG. 3.— (a) Solution grid; dots denote cell centers where the f_{ij} values are defined. Fluxes are defined on the cell boundaries. Thick solid curve is the boundary of the loss cone, $\mathcal{R} = \mathcal{R}_{lc}(\mathcal{E})$. (b) Schematic diagram showing the fluxes associated with grid cell (i, j) . (c) Finite-differencing for grid cells adjacent to (above) the loss cone boundary is affected by the lack of knowledge of f inside the loss cone. In the case of “empty loss cone” boundary conditions, shown here, f is assumed to be zero inside the loss cone (open circles). Cohn-Kulsrud boundary conditions are expressed purely in terms of the values of f near the loss-cone boundary; no derivatives are evaluated there and the values of f inside the loss cone are not needed.

The dimensionless function $q_{lc}(\mathcal{E})$, equation (23), that appears in the Cohn-Kulsrud boundary layer treatment also depends on m_\star/M_\bullet . Since

$$\mathcal{D}(\mathcal{E}) = \Gamma f_0 \mathcal{D}^*(\mathcal{E}^*), \quad (85)$$

we can write

$$q_{lc}(\mathcal{E}^*) = 2\sqrt{2}\pi^2 \ln \Lambda \frac{m_\star}{M_\bullet} \left(\frac{r_m}{r_g}\right)^{\gamma-3} \frac{\mathcal{D}^*(\mathcal{E}^*)}{\mathcal{E}^{*3/2}} \frac{1}{\mathcal{R}_{lc}} \quad (86)$$

where

$$\mathcal{D}^*(\mathcal{E}^*) = \frac{D_{\mathcal{R}\mathcal{R}}^*(\mathcal{E}^*, \mathcal{R}_{lc})}{\mathcal{R}_{lc}} \quad (87)$$

is the dimensionless form of the function defined in equation (24). For instance, in the case that diffusion in L is due only to non-resonant relaxation, equations (86) and (29) imply

$$q_{lc}(\mathcal{E}^*) = \frac{2\sqrt{2}\pi^2}{3} \frac{m_\star}{M_\bullet} \ln \Lambda \left(\frac{r_m}{r_g}\right)^{\gamma-3} \frac{5F_0^* + 12F_3^* - 4F_7^*}{\mathcal{E}^{*5/2} \mathcal{R}_{lc}}. \quad (88)$$

4.2. Basic numerical approach

As in Cohn & Kulsrud (1978), the distribution function f is evaluated at the cell centers while the flux coefficients and fluxes are evaluated at the cell boundaries (Figure 3a). The rate of change of $\mathcal{J}f$ in a cell is then equated to the net flux through the cell boundaries (Figure 3b). The dimensionless evolution equation:

$$\frac{\partial f^*}{\partial t^*} = -\mathcal{J}^{*-1} \beta e^{-Z} \frac{\partial}{\partial Z} (\mathcal{J}^* \phi_{\mathcal{E}}^*) - e^{-X} \frac{\partial}{\partial X} \phi_{\mathcal{R}}^* \quad (89)$$

was written in implicit discrete form, with the time derivative represented as a backwards difference and the flux coefficients evaluated at the previous time step. In discrete form, the $N_X \times N_Z$ difference equations become

$$\frac{f_{ij}^{(n+1)} - f_{ij}^{(n)}}{\Delta t} = \sum_{k=i-1}^{i+1} \sum_{l=j-1}^{j+1} A_{ijkl} f_{kl}^{n+1} \quad (90)$$

where $f_{ij}^{(n)} = f(Z_i, X_j)$ evaluated at the n th time step. Solution of the matrix equation (90) is carried out using the fortran program `f07acf` from *Numerical Algorithms Group*. This routine uses iterative refinement to produce a solution with double-precision accuracy. Iteration was found to be unstable when the time step, Δt , was taken to be too large; the maximum allowable Δt was found to decrease with increasing number of grid cells. Less accurate matrix inversion routines were found to be faster but also more susceptible to instability.

Cohn & Kulsrud (1978) employed a linear grid in \mathcal{R} extending from $\mathcal{R} = 0$ to $\mathcal{R} = 1$. As a result, the dependence of f on \mathcal{R} near the loss cone was not well resolved. The use here of a logarithmic grid in \mathcal{R} yields many more grid points at small \mathcal{R} , permitting a more careful treatment of the solution near the loss cone, as discussed below.

4.3. Boundary conditions

Two choices for the the boundary condition at small \mathcal{R} are implemented. The simplest is an “empty loss cone” (ELC) condition: $f(\mathcal{E}, \mathcal{R}) = 0$ for $\mathcal{R} \leq \mathcal{R}_{lc}(\mathcal{E})$. To implement this condition, cells that contain the curve $\mathcal{R} = \mathcal{R}_{lc}(\mathcal{E})$ and for which the cell center is outside the loss cone (“loss-cone cells”) are identified, and for these cells, a record is made of the adjacent cells for which the cell center is inside the loss cone, i.e. for which $\mathcal{R}_{ij} < \mathcal{R}(\mathcal{E}_{ij})$. There are nine possible combinations of adjacent cells for which this condition can be satisfied; Figure 3c illustrates the most common, consisting of three adjacent cells. The finite-difference expressions for the flux derivatives in the loss-cone cells are written with the appropriate f_{ij} -values set to zero.

The second choice of small- \mathcal{R} boundary condition was based on the Cohn-Kulsrud (1978) boundary layer solution. In the spirit of that derivation, the evolution equations near the loss cone boundary are first simplified by ignoring the contribution of gradients in \mathcal{E} to the flux, which allows equations (17) to be written as

$$\phi_{\mathcal{E}} = -D_{\mathcal{E}\mathcal{R}} \frac{\partial f}{\partial \mathcal{R}} - D_{\mathcal{E}} f, \quad \phi_{\mathcal{R}} = -D_{\mathcal{R}\mathcal{R}} \frac{\partial f}{\partial \mathcal{R}} - D_{\mathcal{R}} f. \quad (91)$$

In the Cohn-Kulsrud solution, the \mathcal{R} -directed flux per unit of \mathcal{E} across the loss cone boundary:

$$F(\mathcal{E}) = - \int_{\mathcal{R}_{lc}}^1 \left(-\mathcal{J} \frac{\partial \phi_{\mathcal{R}}}{\partial \mathcal{R}} \right) d\mathcal{R} = \mathcal{J}(\mathcal{E}) [\phi_{\mathcal{R}}(\mathcal{R} = 1) - \phi_{\mathcal{R}}(\mathcal{R} = \mathcal{R}_{lc})] = -\mathcal{J}(\mathcal{E}) \phi_{\mathcal{R}}(\mathcal{R}_{lc}) \quad (92)$$

is given by

$$F(\mathcal{E}) = 4\pi^2 L_c^2(\mathcal{E}) \mathcal{R}_{lc}(\mathcal{E}) f(\mathcal{E}, \mathcal{R}_{lc}) \xi(q_{lc}) \quad (93)$$

where

$$\xi(x) \equiv 1 - 4 \sum_{m=1}^{\infty} \frac{e^{-\alpha_m^2 x/4}}{\alpha_m^2} \quad (94)$$

and the α_m are the consecutive zeros of the Bessel function $J_0(\alpha)$ (Merritt 2013, equations 6.58-6.62). Thus

$$\phi_{\mathcal{R}}(\mathcal{E}, \mathcal{R}_{lc}) = -\frac{\sqrt{2}}{\pi} \frac{\mathcal{E}^{3/2}}{GM_{\bullet}} \mathcal{R}_{lc}(\mathcal{E}) f_{lc}(\mathcal{E}) \xi(q_{lc}) \quad (95)$$

where $f_{lc}(\mathcal{E}) \equiv f(\mathcal{E}, \mathcal{R}_{lc})$. The gradient in f at $\mathcal{R} = \mathcal{R}_{lc}$ in the Cohn-Kulsrud solution is

$$\left(\frac{\partial f}{\partial \mathcal{R}} \right)_{lc} = \frac{\xi}{q_{lc}} \frac{f_{lc}}{\mathcal{R}_{lc}} \quad (96)$$

which is inserted into the first of equations (91) to give the flux in \mathcal{E} :

$$\phi_{\mathcal{E}}(\mathcal{E}, \mathcal{R}_{lc}) = -D_{\mathcal{E}\mathcal{R}}(\mathcal{E}, \mathcal{R}_{lc}) \frac{\xi}{q_{lc}} \frac{f_{lc}(\mathcal{E})}{\mathcal{R}_{lc}(\mathcal{E})} - D_{\mathcal{E}}(\mathcal{E}, \mathcal{R}_{lc}) f_{lc}(\mathcal{E}). \quad (97)$$

Equations (95) and (97) are the adopted boundary conditions. These expressions are applied at the inner edges of any loss-cone cell, while the general expressions (17) for the flux are applied on the outer edges of those cells.

The summation in equation (94) is slowly converging when q is small (Figure 4a). An approximate expression is

$$\xi_{\text{approx}}(x) = \frac{x}{(x^2 + x^4)^{1/4}} \quad (98)$$

for which the relative error is $\sim 1\%$ at all $q \lesssim 1$ and tends to zero for large q_{lc} (Figure 4b). Equation (98) was adopted for the code.

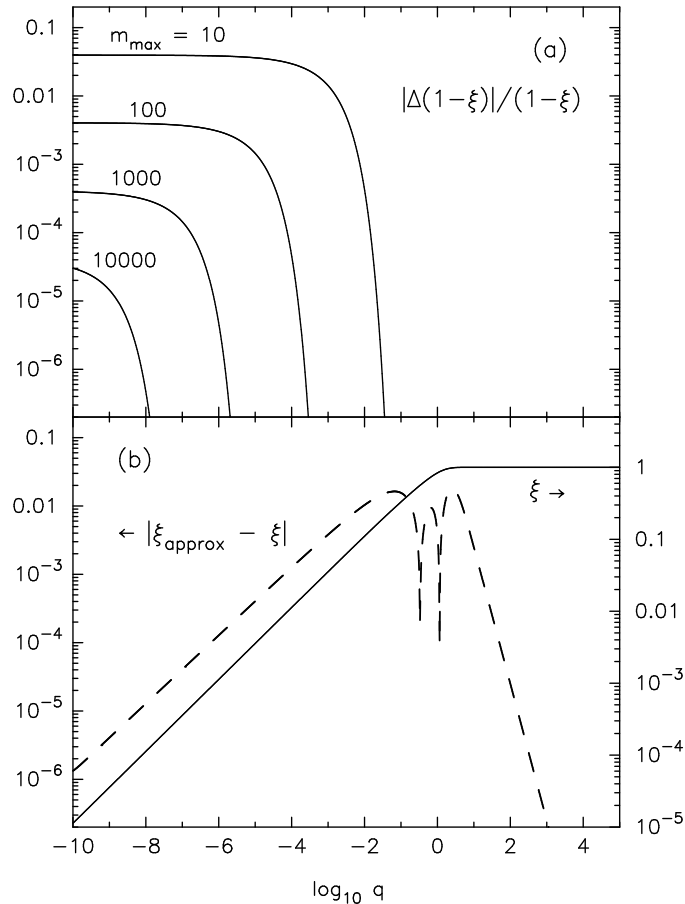


FIG. 4.— (a) Convergence of the series in equation (94). Each curve is labelled by m_{\max} , the number of terms included in the summation; the ordinate is the relative error. (b) Solid curve shows $\xi(q)$ computed from equation (94) using 10^5 terms. Dashed curve is the absolute error in the approximate expression (98).

Note that the values f_{ij} corresponding to grid cells inside the loss cone are not used and therefore are not advanced in time. Indeed in this region, f is not expected to satisfy Jeans’s theorem and a proper treatment would require inclusion of $r-$ as an additional independent variable.

The boundary condition at $\mathcal{R} = 1$ is $\phi_{\mathcal{R}} = 0$.

Two possibilities were implemented for the boundary condition at small \mathcal{E} , i.e. far from the SBH. The first consists of fixing $f(\mathcal{E}_{\min}, \mathcal{R})$ at its initial value. Cohn & Kulsrud (1978) implemented a similar boundary condition. This choice implies a nonzero flux of stars into the region of integration, although that flux can be very small if \mathcal{E}_{\min} is small. The second choice consists of setting to zero the $\mathcal{E}-$ directed flux at $\mathcal{E} = \mathcal{E}_{\min}$, i.e. requiring

$$D_{\mathcal{E}\mathcal{E}} \frac{\partial f}{\partial \mathcal{E}} = -D_{\mathcal{E}\mathcal{R}} \frac{\partial f}{\partial \mathcal{R}} - D_{\mathcal{E}} f, \quad \mathcal{E} = \mathcal{E}_{\min}. \quad (99)$$

This boundary condition is more in keeping with N -body simulations that have a fixed number of stars. The “zero-flux” boundary condition is implemented as follows. (1) At each time step, inversion of the matrix A_{ijkl} is first carried out specifying no change at $\mathcal{E} = \mathcal{E}_{\min}$, i.e., $Z = Z_{NZ}$. (2) Equation (99) is then used to solve for $f(Z_{NZ}, X_j)$, $j = 1, \dots, NX$. In this step, derivatives are expressed in terms of the unknown values of f at Z_{NZ} and the just-computed values at Z_{NZ-1} , allowing solution of f by inversion of a tri-diagonal matrix.

4.4. Initial conditions

The initial $f(\mathcal{E}, \mathcal{R})$ was typically based on an isotropic power-law model, equation (80), but with a modified \mathcal{R} -dependence to account for the presence of the loss cone. The simplest choice is to set $f = 0$ for $\mathcal{R} \leq \mathcal{R}_{lc}$. A more natural choice is to set the initial f to

$$\begin{aligned} f(\mathcal{E}, \mathcal{R}) &= f(\mathcal{E}, 1) \frac{\ln(\mathcal{R}/\mathcal{R}_{lc})}{\ln(1/\mathcal{R}_{lc})}, & \mathcal{R} > \mathcal{R}_{lc} \\ &= 0, & \mathcal{R} \leq \mathcal{R}_{lc} \end{aligned} \quad (100)$$

which is the approximate (small- \mathcal{R}) steady-state solution for an empty loss cone. Other choices for the initial conditions are described below.

5. EXAMPLES

Subsequent papers in this series will describe the evolution of $f(E, L)$ due to the various physical mechanisms represented above. Here we use the algorithm to explore some simple dependencies of the classical Bahcall-Wolf solution on m_*/M_\bullet , and on time.

5.1. Models with classical diffusion coefficients; empty loss cone

The number of parameters that define an integration can be minimized by assuming empty-loss-cone (ELC) boundary conditions, and adopting the classical (CK) diffusion coefficients. The stellar mass, m_* , then appears only in expressions like (78) that set the scaling of the time or density, and any initial $f(\mathcal{E}, \mathcal{R})$ should evolve to the same equilibrium f modulo a known scaling in amplitude. Furthermore this steady state should be similar to the Bahcall-Wolf “zero-flux” model, $n \sim r^{-7/4}$, $f \sim \mathcal{E}^{1/4}$; the differences being due to the fact that those authors assumed $f = f(\mathcal{E}, t)$ and allowed loss of stars to the SBH only via diffusion in energy.

The code was tested under these assumptions, starting from power-law models like those of equation (80) and various values of γ . The isotropic models were modified initially as in equation (100) so that f fell to zero at $\mathcal{R} = \mathcal{R}_{lc}$; the ELC boundary conditions then guaranteed that $f(\mathcal{R}_{lc})$ remained zero at all $\mathcal{R} \leq \mathcal{R}_{lc}$. $f(\mathcal{E}_{min}, \mathcal{R})$ was fixed to its initial form.

It is permissible and convenient to scale these models by assuming that the final mass density has a specified value at a specified radius. Let that radius be αr_g and let the density at that radius be $\rho(\alpha r_g)$. It may be shown, using equation (78), that the elapsed time is then given in terms of the dimensionless time t^* by

$$\begin{aligned} t &= \frac{1}{4\pi \ln \Lambda} \left(\frac{M_\bullet}{m_*} \right) \left(\frac{r_g}{c} \right) \left[\frac{\rho(\alpha r_g) r_g^3}{M_\bullet} \right]^{-1} n^*(\alpha) t^* \\ &\approx 7.4 \times 10^{17} \left(\frac{\ln \Lambda}{15} \right)^{-1} \left(\frac{M_\bullet/m_*}{10^5} \right) \left(\frac{M_\bullet}{10^6 M_\odot} \right)^{-1} \left[\frac{\rho(\alpha r_g)}{10^6 M_\odot \text{pc}^{-3}} \right]^{-1} n^*(\alpha) t^* \text{ yr} \end{aligned} \quad (101)$$

where $n^*(\alpha)$ is the final, dimensionless model density (cf. equation 81) at $r = \alpha r_g$, i.e. at $r^* = \alpha$. The loss rate, equation (84), can similarly be related to the dimensionless loss rate as

$$\begin{aligned} \frac{dN}{dt} &= 4\pi \ln \Lambda \left(\frac{c}{r_g} \right) \left[\frac{\rho(\alpha r_g) r_g^3}{M_\bullet^2} \right]^2 \frac{1}{n^*(\alpha)^2} \frac{dN^*}{dt^*} \\ &\approx 1.49 \times 10^{-35} \left(\frac{\ln \Lambda}{15} \right) \left(\frac{M_\bullet}{10^6 M_\odot} \right)^3 \left[\frac{\rho(\alpha r_g)}{10^6 M_\odot \text{pc}^{-3}} \right]^2 \frac{1}{n^*(\alpha)^2} \frac{dN^*}{dt^*} \text{ yr}^{-1}. \end{aligned} \quad (102)$$

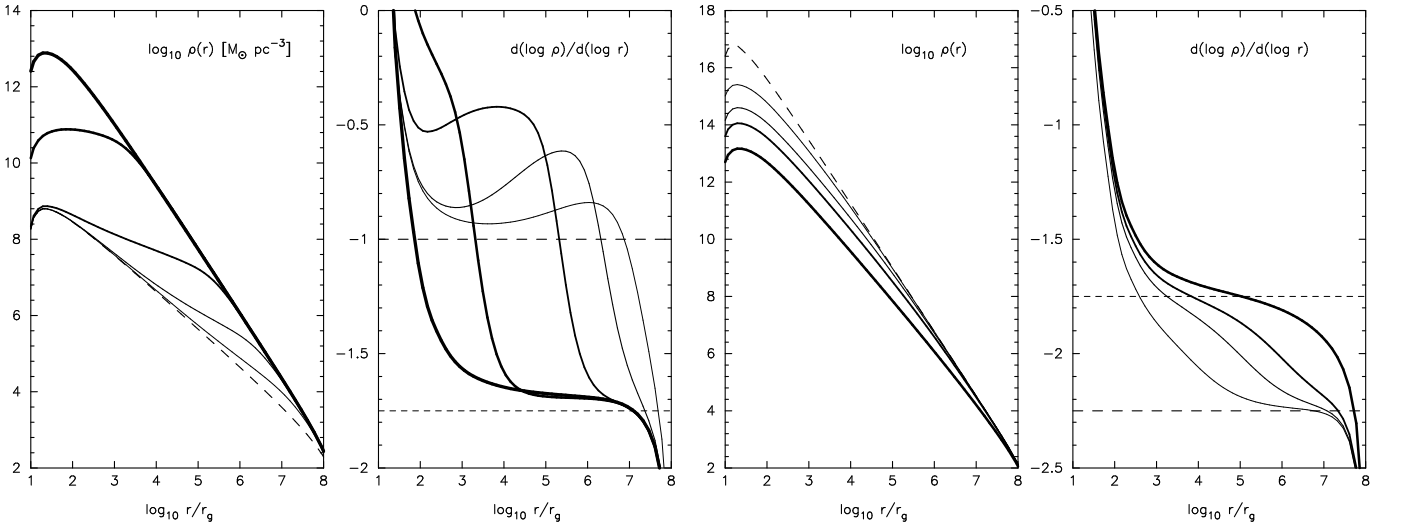


FIG. 5.— Evolution due to classical relaxation of two models assuming empty-loss-cone (ELC) boundary conditions. The initial model had $n \sim r^{-1}$ (left) and $n \sim r^{-9/4}$ (right), shown as the dashed lines. Other curves are at times $(1, 2, 3, 4, 5) \times 10^9$ yr (left) and $(0.01, 0.1, 0.5, 7) \times 10^8$ yr (right) based on the scaling described in the text; line thickness increases with time. Dotted lines show $d \log \rho / d \log r = -7/4$, the Bahcall-Wolf slope.

Figure 5 shows the evolution of $\rho(r)$ for integrations with $\gamma = 1$ and $\gamma = 9/4$. The units of time and density were fixed by assuming a final density at $10^6 r_g$ of $10^6 M_\odot \text{pc}^{-3}$; the other parameters were set to the fiducial values in

equations (101) and (102), e.g. $M_\bullet = 10^6 M_\odot$, hence $10^6 r_g \approx 4.8 \times 10^{-2}$ pc; the radius containing a mass in stars of $2M_\bullet$ at the final time step, the “gravitational influence radius,” is $\sim 3 \times 10^8 r_g$, roughly equal to the outer radius of the solution grid. In the model with initially shallower slope ($\gamma = 1$), the density evolves “from the outside in” toward the steady state, while in the model with $\gamma = 9/4$ the density evolves at all radii at roughly the same rate.

The final density profile is the same in these two models, as expected, and is close to a power law:

$$\rho(r) \sim r^{-\delta}, \quad 1.65 \lesssim \delta \lesssim 1.70 \quad (103)$$

at $10^4 r_g \leq r \leq 10^7 r_g$. This is slightly shallower than the canonical $\rho \sim r^{-1.75}$ of the Bahcall-Wolf solution. The difference can be attributed to the depletion of orbits in the loss cone, the effects of which are progressively more severe at energies close to the SBH.

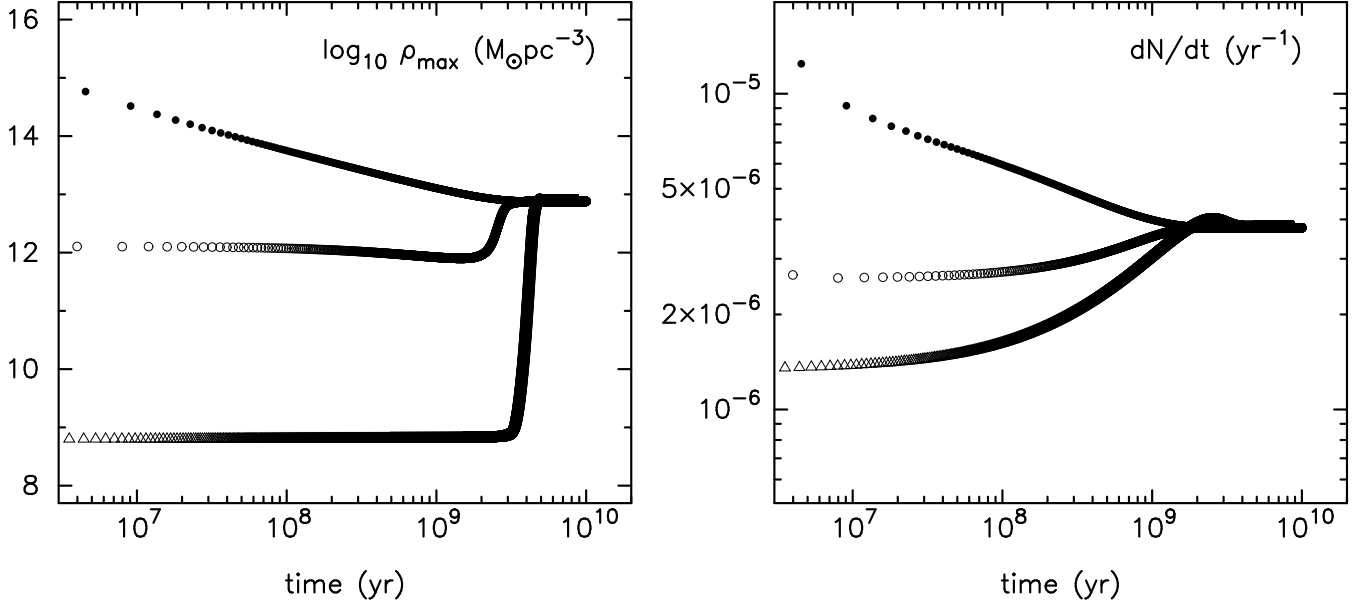


FIG. 6.— Evolution of the peak density (left) and of the total loss rate (right) for three integrations assuming classical diffusion coefficients and ELC boundary conditions. The initial density slope was $\gamma = 1$ (triangles), $\gamma = 1.5$ (open circles), and $\gamma = 2$ (filled circles). Scaling assumes a final density at $10^6 r_g$ of $10^6 M_\odot \text{ pc}^{-3}$.

Figure 6 shows the evolution of the peak (\sim central) density, as well as the total loss rate \dot{N} , for three integrations starting from $\gamma = \{1, 3/2, 2\}$. In each case a steady state is reached in a time of $\sim 5 \times 10^9$ yr. This can be compared to the classical relaxation time, a standard expression for which is

$$\begin{aligned} T_r(r) &= \frac{0.34\sigma^3}{G^2 m \rho \ln \Lambda} \\ &\approx 0.95 \times 10^{10} \left(\frac{\sigma}{200 \text{ km s}^{-1}} \right)^3 \left(\frac{\rho}{10^6 M_\odot \text{ pc}^{-3}} \right)^{-1} \left(\frac{m_\star}{M_\odot} \right)^{-1} \left(\frac{\ln \Lambda}{15} \right)^{-1} \text{ yr} \end{aligned} \quad (104)$$

(Merritt 2013, Eq. 3.1). Evaluating equation (104) in the *final* model, assuming $n(r) \sim r^{-1.7}$, $m_\star = 10^{-5} M_\bullet = 10 M_\odot$, $\ln \Lambda = 15$, and

$$\sigma(r) \approx \left[\frac{1}{1+\gamma} \frac{GM_\bullet}{r} \right]^{1/2} \approx 183 \left(\frac{r}{10^6 r_g} \right)^{-1/2} \text{ km s}^{-1}, \quad (105)$$

yields

$$T_r(r) \approx 7 \times 10^9 \left(\frac{r}{10^6 r_g} \right)^{0.20} \text{ yr}, \quad (106)$$

consistent with the observed equilibration time.

5.2. Models with classical diffusion coefficients; Cohn-Kulsrud loss cone

The simple rescaling defined in the previous section no longer works when adopting the Cohn-Kulsrud (CK) loss-cone boundary conditions, equations (95) – (97), since the dimensionless function $q_{lc}(\mathcal{E}, t)$ depends separately on the factor

$$\frac{m_\star}{M_\bullet} \ln \Lambda \quad (107)$$

(equations 23, 88). Two models with different initial f 's will not necessarily arrive at steady states that are rescaled versions of one another unless the final $q_{lc}(\mathcal{E})$ happens also to be the same.

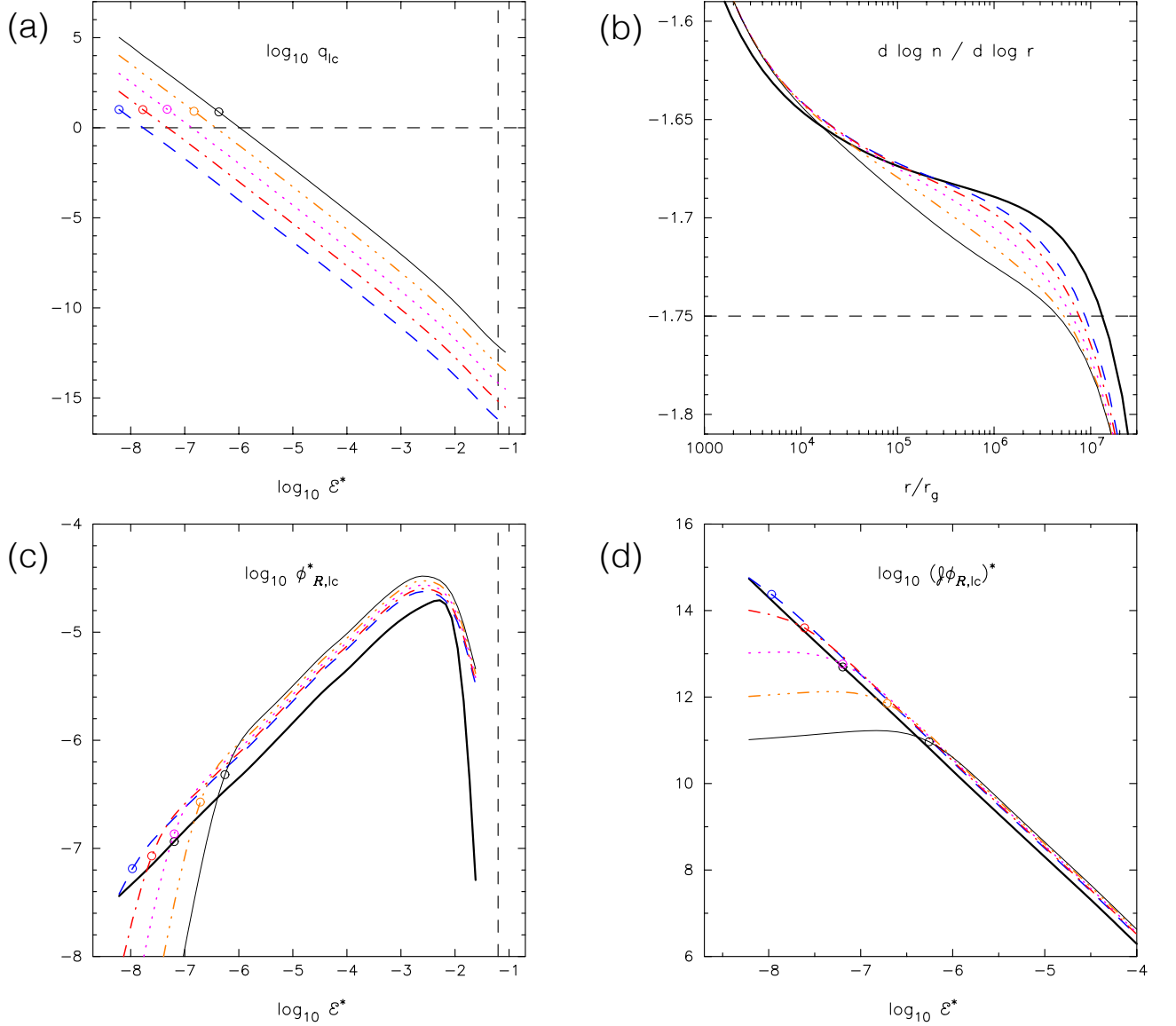


FIG. 7.— Final quantities for a set of integrations adopting the Cohn-Kulsrud (CK) boundary conditions, classical diffusion coefficients, and various values of m_*/M_\bullet . Thick solid (black): $q_{lc} = 0$ (empty loss cone; (b)-(d) only); dashed (blue): $m_*/M_\bullet = 10^{-7}$; dot-dashed (red): 10^{-6} ; dotted (purple): 10^{-5} ; dash-dot-dot (orange): 10^{-4} ; thin solid (black): 10^{-3} . Open circles mark the energy where $q_{lc} = |\ln \mathcal{R}_{lc}|$, roughly the expected energy of transition between the empty- and full-loss-cone regimes.

Differences in scaling will be minimized if the initial model is close to the final model. In this section, initial conditions are chosen to be close to the Bahcall-Wolf form, $f \sim \mathcal{E}^{1/4}$. Differences in the final state will be due to differences in the value of (107), i.e. to differing degrees of loss-cone “fullness”. Parameters common to all the integrations in this section were

$$\gamma = 7/4, \quad \frac{r_m}{r_g} = 10^9, \quad \ln \Lambda = 15. \quad (108)$$

Various values were adopted for m_*/M_\bullet , implying different forms for $q_{lc}(\mathcal{E}, t = 0)$. The initial density profile is

approximately

$$\begin{aligned}\rho(r) &\approx \frac{3-\gamma}{2\pi} \frac{M_\bullet}{r_m^3} \left(\frac{r}{r_m}\right)^{-\gamma} \\ &\approx 2.0 \times 10^2 \left(\frac{M_\bullet}{10^6 M_\odot}\right) \left(\frac{r_m}{10 \text{ pc}}\right)^{-3} \left(\frac{r}{r_m}\right)^{-7/4} M_\odot \text{pc}^{-3}\end{aligned}\quad (109)$$

and the unit of time becomes

$$[t] \approx 3.0 \times 10^7 \left(\frac{M_\bullet/m_\star}{10^5}\right) \text{ yr}.\quad (110)$$

These initial models are expected to reach steady states characterized by

$$f(\mathcal{R}) \sim \frac{f(1)}{\ln(1/\mathcal{R}_{\text{lc}})} \ln\left(\frac{\mathcal{R}}{\mathcal{R}_{\text{lc}}}\right)\quad (111)$$

for $q_{\text{lc}} \ll 1$ (“empty loss cone”) and

$$f(\mathcal{R}) \sim \text{const}.\quad (112)$$

for $q_{\text{lc}} \gg 1$ (“full loss cone”).

Figure 7 plots four dimensionless quantities associated with the steady-state solutions.

(a) $q_{\text{lc}}(\mathcal{E})$. The transition from empty- ($q_{\text{lc}} \ll 1$) to full- ($q_{\text{lc}} \gg 1$) loss-cone regimes takes place at progressively larger binding energies, i.e. smaller radii, as m_\star is increased. For the smallest value of m_\star adopted here ($m_\star/M_\bullet = 10^{-7}$) the final model is essentially in the empty-loss-cone regime everywhere.

(b) The logarithmic derivative of the configuration-space density, $d \log n / d \log r$. At intermediate radii, $10^4 \lesssim r/r_g \lesssim 10^7$, the slope is close to -1.7 in all final models, slightly shallower than in the (isotropic, scale-free) Bahcall-Wolf solution. This is due to the progressive depletion of the loss cone near the SBH, as in the ELC examples above. That depletion becomes less severe as m_\star and hence q_{lc} are increased and the slope in the models with the largest m_\star approaches most closely to $-7/4$.

(c) The magnitude of the \mathcal{R} -directed flux, $\phi_{\mathcal{R}} = -D_{\mathcal{R}\mathcal{R}}(\partial f / \partial \mathcal{R}) - D_{\mathcal{R}} f$, evaluated at $\mathcal{R} = \mathcal{R}_{\text{lc}}(\mathcal{E})$. The empty-loss-cone model exhibits an approximate power-law dependence, $\phi_{\mathcal{R},\text{lc}} \sim \mathcal{E}^{*1/2}$, at small \mathcal{E}^* (large radius). In the models with finite m_\star , the flux drops sharply beyond the energy where $q_{\text{lc}}(\mathcal{E}) \sim \ln \mathcal{R}_{\text{lc}}$.

(d) The quantity $\mathcal{J}(\mathcal{E})\phi_{\mathcal{R},\text{lc}}(\mathcal{E})$, whose integral $d\mathcal{E}$ is proportional to the integrated loss rate. Since $\mathcal{J} \propto \mathcal{E}^{-5/2}$, $\mathcal{J}\phi_{\mathcal{R},\text{lc}} \sim \mathcal{E}^{-2}$ for small \mathcal{E} in the empty-loss-cone model, implying an integrated loss rate that diverges as $\mathcal{E}^{-1} \sim r$. When m_\star is non-zero, $\mathcal{J}\phi_{\mathcal{R},\text{lc}}$ instead “levels out” roughly where $q_{\text{lc}} \sim |\ln \mathcal{R}_{\text{lc}}|$, implying a finite total loss rate.

Equation (84), together with the parameters (108), yields a relation between the dimensional and dimensionless loss rates:

$$\frac{dN(< r)}{dt} = 4\pi \ln \Lambda \frac{c}{r_g} \left(\frac{r_m}{r_g}\right)^{2(\gamma-3)} \frac{dN^*(< r^*)}{dt^*} \approx 3.8 \times 10^{-14} \left(\frac{M_\bullet}{10^6 M_\odot}\right)^{-1} \frac{dN^*}{dt^*} \text{ yr}^{-1}.\quad (113)$$

Figure 8a plots this function, at the final time, for the five models with non-zero q_{lc} , assuming $M_\bullet = 10^6 M_\odot$. We can compare these loss rates to those predicted by a simple model based on the assumption of an empty loss cone (Merritt 2013, equation 6.91):

$$\dot{N}(< r) \approx \frac{4\pi}{\ln \mathcal{R}_{\text{lc}}} \int^r \frac{n(r)}{T_r(r)} r^2 dr\quad (114a)$$

$$\approx \frac{3}{4\pi} \frac{(1+\gamma)^{3/2}(3-\gamma)^2}{(9/2-2\gamma)} \frac{N(< r_m)^2 G^{1/2} m_\star^2 \ln \Lambda}{M_\bullet^{3/2} r_m^{3/2} \ln \mathcal{R}_{\text{lc}}} \left(\frac{r}{r_m}\right)^{9/2-2\gamma}\quad (114b)$$

$$\approx 3.4 \frac{\ln \Lambda}{\ln \mathcal{R}_{\text{lc}}} \sqrt{\frac{GM_\bullet}{r_m^3}} \frac{r}{r_m}\quad (114c)$$

$$\approx 5.6 \times 10^{-7} \left(\frac{M_\bullet}{10^6 M_\odot}\right)^{-1} \frac{r}{r_m} \text{ yr}^{-1}.\quad (114d)$$

(The second line follows from equations (104) and (109); the third line sets $\gamma = 7/4$; and the final line uses the parameters (108) and approximates \mathcal{R}_{lc} by $r_{\text{lc}}/r_m = 8r_g/r_m$.) Recalling that $r_m/r_g = 10^9$ for the models of Figure 8, we see that equation (114) correctly predicts the loss rates in the Fokker-Planck models for the case of small m_\star/M_\bullet , i.e. in the $q_{\text{lc}} \rightarrow 0$ limit. In the case of an empty loss cone, there is a (linear) divergence of the integrated loss rate with r ; when m_\star is finite, there is a transition to the $q_{\text{lc}} > 1$ regime in which the loss rate is given approximately by

$$\dot{N}(< r) \approx 4\pi \int_{r_{\text{crit}}}^r \frac{n(r)}{P(r)} \mathcal{R}_{\text{lc}}(r) r^2 dr\quad (115)$$

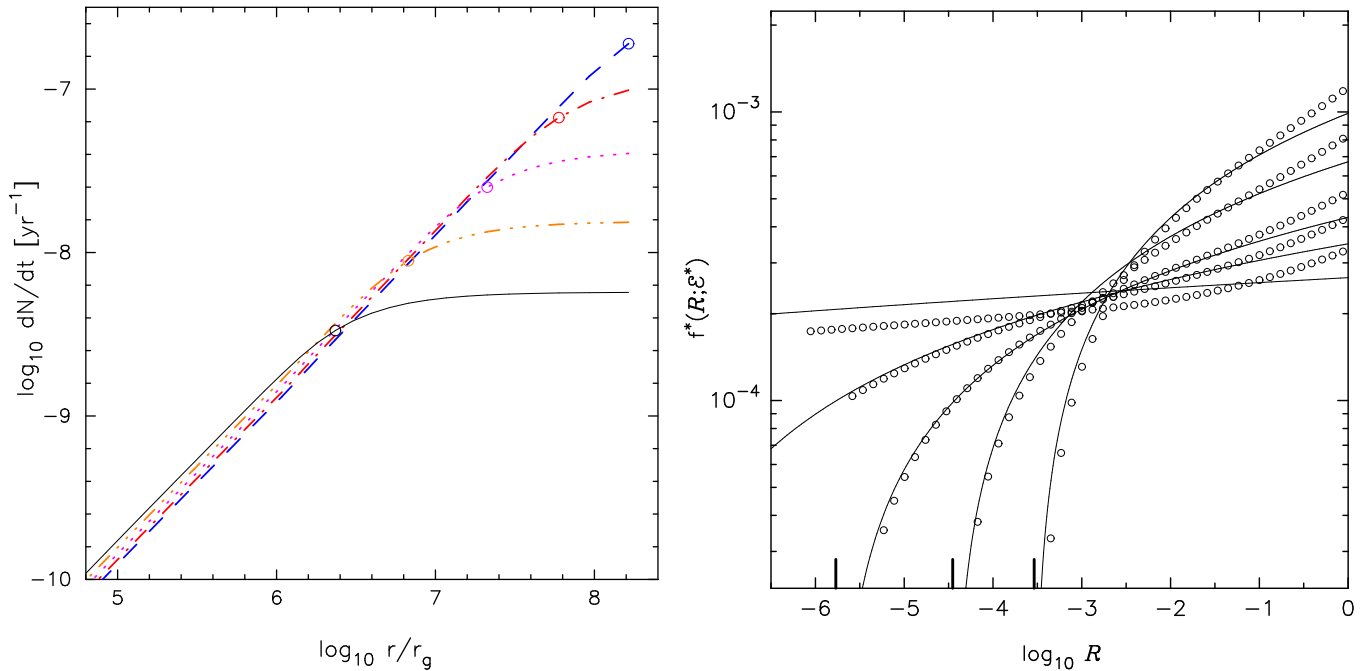


FIG. 8.— **Left panel.** Dimensional loss rate, defined as number of stars per year scattered into the SBH from radii smaller than r , for the five models of Figure 7. “Radius” here means $GM_{\bullet}/(2\mathcal{E})$ and $M_{\bullet} = 10^6 M_{\odot}$ has been assumed. Line colors and types have the same meanings as in Figure 7. Circles indicate the radii where $q_{lc} = |\ln \mathcal{R}_{lc}|$. **Right panel.** \mathcal{R} -dependence of f in the steady-state model from Figure 7 with $m_{\star}/M_{\bullet} = 10^{-5}$ (NR diffusion coefficients). Circles are $f(\mathcal{R}; \mathcal{E})$ at five values of \mathcal{E} , for which $q_{lc}(\mathcal{E}) \approx \{45.4, 5.44, 0.816, 6.89 \times 10^{-3}, 6.14 \times 10^{-5}\}$. Curves are equations (117), after normalizing such that the number of stars at each \mathcal{E} is the same in the numerical and analytic models. The vertical tick-marks at three values of \mathcal{R} show $\mathcal{R}_0(\mathcal{E})$, equation (118).

where r_{crit} is the smallest radius for which q_{lc} exceeds one (Merritt 2013, equation 6.91). For these models, equation (115) predicts a contribution from the full-loss-cone regimes that scales with radius as

$$\dot{N}(< r) \propto r_{\text{crit}}^{-5/4} - r^{-5/4}, \quad r > r_{\text{crit}} \quad (116)$$

consistent with the “leveling out” of the curves in Figure 8 at radii greater than $\sim r_{\text{crit}}$.

It is interesting to compare the \mathcal{R} -dependence of f in the final models with the form that is often assumed when computing loss rates (e.g. Magorrian & Tremaine 1998):

$$f(\mathcal{R}) = f(\mathcal{R}_{lc}) + \frac{f(1) - f(\mathcal{R}_{lc})}{\ln(1/\mathcal{R}_{lc})} \ln(\mathcal{R}/\mathcal{R}_{lc}), \quad \mathcal{R}_{lc} \leq \mathcal{R} \leq 1, \quad (117a)$$

$$f(\mathcal{R}_{lc}) = \frac{f(1)}{1 + q_{lc}^{-1} \xi(q) \ln(1/\mathcal{R}_{lc})} \quad (117b)$$

Equation (117a) is a steady-state (constant flux) solution of the diffusion equation in \mathcal{R} if the low- \mathcal{R} forms of the diffusion coefficients are used, and equation (117b) follows from the Cohn-Kulsrud treatment (as given in Merritt 2013, equations (6.59), (6.61)). Figure 8b plots $f(\mathcal{R})$, at various \mathcal{E} , in the final model from the integration with $m_{\star}/M_{\bullet} = 10^{-5}$. Equations (117) are overplotted, after normalizing to give the same total number at each \mathcal{E} . The agreement is reasonably good, verifying that the boundary conditions have been correctly implemented. But the dependence of f on \mathcal{R} near $\mathcal{R} = 1$ deviates from the simple logarithmic form of equation (117a), due to the fact that the correct – not small- \mathcal{R} asymptotic – forms of the diffusion coefficients are used in the numerical code.

In the case of a non-empty loss cone, the $f = 0$ intercept of the “external” ($\mathcal{R} > \mathcal{R}_{lc}$) solution occurs at $\mathcal{R} = \mathcal{R}_0 < \mathcal{R}_{lc}$, where

$$\mathcal{R}_0(q_{lc}) = \mathcal{R}_{lc}(\mathcal{E}) e^{-q_{lc}/\xi(q_{lc})} \quad (118)$$

(Merritt 2013, equation 6.65). In Figure 8b, \mathcal{R}_0 as given by equation (118) is indicated by vertical marks, and appears quite consistent with the value of \mathcal{R} at which the numerical solutions are tending to zero.

5.3. Models with classical and resonant diffusion coefficients

The form of steady-state solutions derived in the preceding two sections depended on the value assumed for the stellar mass m_{\star} , insofar as m_{\star} determines q_{lc} . But the dependence was found to be weak, and all of the steady-state solutions could be rescaled in f and \mathcal{E} to approximately the same $\bar{f}(\mathcal{E})$.

This scale-free property is lost if the resonant relaxation diffusion terms are included. Sufficiently near the SBH, changes in angular momentum will be dominated by resonant relaxation while changes in energy will still be dominated

by the classical diffusion coefficients. A characteristic radius appears: the distance, r_{eq} , from the SBH at which the timescale for changes in L due to resonant relaxation is the same as the timescale for changes in L due to classical relaxation. That radius is given roughly by the solution to

$$m_{\star}N(< r_{\text{eq}}) = A_{\text{NR}}M_{\bullet}, \quad A_{\text{NR}} = \frac{0.68}{(3-\gamma)(1+\gamma)^{3/2}} \frac{1}{\log \Lambda} \quad (119)$$

(Merritt 2013, Equation 5.243). Here $N(< r)$ is the number of stars within a sphere of radius r and $t_{\text{coh}} = t_{\text{coh},\text{M}}$ has been assumed; the expression for A_{NR} additionally assumes $n(r) \propto r^{-\gamma}$. Setting $\log \Lambda = 15$, the enclosed (stellar) mass at r_{eq} works out to be $\sim 10^{-2}M_{\bullet}$ for all $0.5 \leq \gamma \leq 2.0$.

Consider a star whose energy diffuses below $E_{\text{eq}} \sim -GM_{\bullet}/r_{\text{eq}}$. The timescale for diffusion in L will suddenly decrease, and the star will be lost to the SBH, in a time much less than the characteristic time for changes in E . A steady state will eventually be reached, but only after $|\partial f/\partial E|$ at $E \sim E_{\text{eq}}$ becomes large enough to drive a flux in E (due to classical relaxation) that equals the flux in L (due to resonant relaxation). The expected result is a depletion in f at $E \sim E_{\text{eq}}$ and a low configuration-space density at $r \lesssim r_{\text{eq}}$ – a “core”.

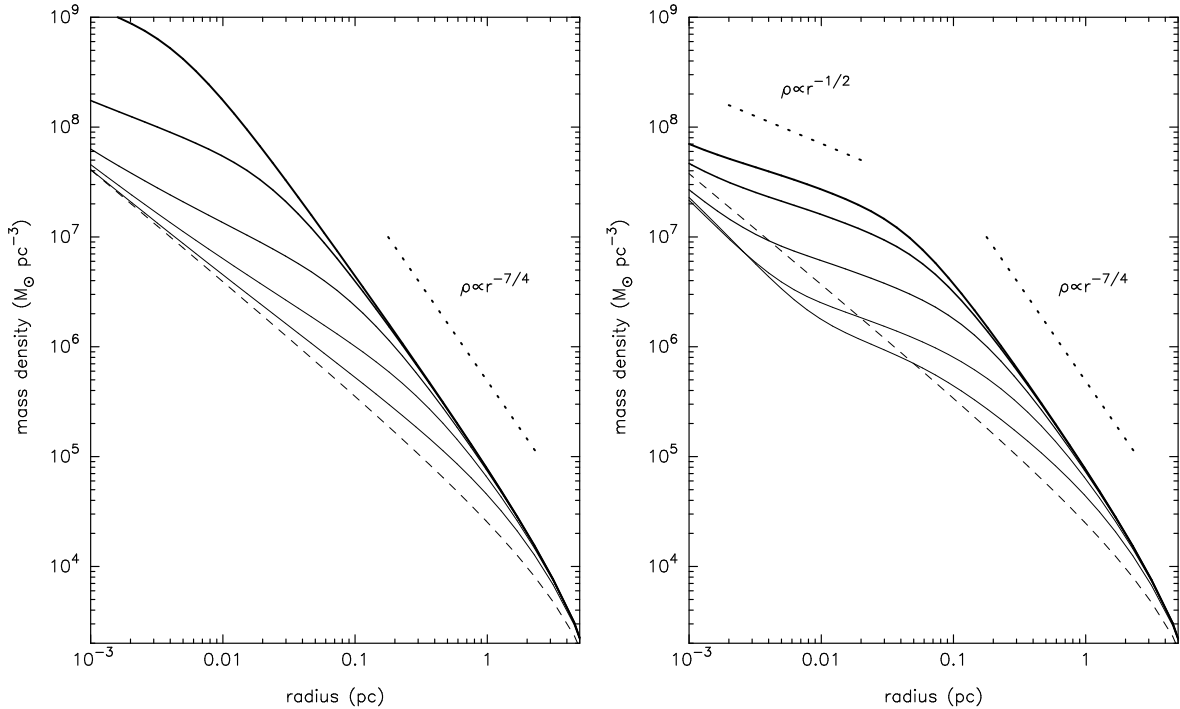


FIG. 9.— Evolution of $\rho(r)$ in two models with the same initial density, $\rho(r) \propto r^{-1}$. **Left:** classical diffusion coefficients were used. **Right:** resonant relaxation terms were included as well. Other features of the integrations are specified in the text; the adopted parameters are appropriate for the nuclear cluster of the Milky Way, with $M_{\bullet} = 4.0 \times 10^6 M_{\odot}$. Densities are plotted at times $t = \{0, 2, 4, 6, 8, 10\} \times 10^9$ yr. The $t = 0$ model is shown by dashed lines, and line width increases with time. Dotted lines show the Bahcall-Wolf slope, $d \log \rho / d \log r = -7/4$, and the slope corresponding to a sharply truncated $f(\mathcal{E})$, $d \log \rho / d \log r = -1/2$. Both models have an integrated stellar mass, within one parsec, of approximately $1.0 \times 10^6 M_{\odot}$ at $t = 5 \times 10^9$ yr, consistent with the mass measured in the Milky Way nuclear cluster (Schödel et al. 2009).

Figure 9 shows the evolution of $\rho(r)$ in two integrations: the first using the classical diffusion coefficients, the second including the resonant-relaxation coefficients as well. Both integrations adopted parameters appropriate for the nuclear cluster of the Milky Way. The quantity $(m_{\star}/M_{\bullet}) \ln \Lambda$ that appears in equation (88) for q_{lc} :

$$\frac{m_{\star}}{M_{\bullet}} \ln \Lambda = 3.75 \times 10^{-6} \left(\frac{m_{\star}}{1 M_{\odot}} \right) \left(\frac{M_{\bullet}}{4 \times 10^6 M_{\odot}} \right)^{-1} \left(\frac{\ln \Lambda}{15} \right) \quad (120)$$

was set to 3.75×10^{-6} , and the radius of the loss sphere, which for a main-sequence star is the tidal disruption radius:

$$r_{\text{lc}} \approx 0.7 \text{ AU} \frac{R_{\star}}{R_{\odot}} \left(\frac{M_{\bullet}}{m_{\star}} \frac{1}{4 \times 10^6} \right)^{1/3} \quad (121)$$

was set to 0.7 AU. These choices were motivated by the fact that the main-sequence turnoff mass in the Galactic center is $\sim 1 M_{\odot}$, and the red giants that are believed to dominate the number counts of the “late-type” stars probably have roughly this mass (Dale et al. 2009). (Due to the relative shortness of the red giant evolutionary phase, most stars are

expected to be disrupted while still on or near the main sequence (MacLeod et al. 2012)). These choices determined the location and flux at the loss-cone boundary via the expressions (95), (97).

The initial density normalization was chosen, after some trial and error, to give an integrated mass within 1 pc of $\sim 1.0 \times 10^6 M_\odot$ at $t = 5 \times 10^9$ yr. This is roughly the value inferred from dynamical analyses of stellar velocities (Schödel et al. 2009).

Figure 9 shows that the integration based on the classical diffusion coefficients nearly reaches the $\rho \propto r^{-7/4}$ Bahcall-Wolf form after 10 Gyr. Deviations from that form are apparent inside ~ 0.01 pc even at this late time; however seen from the Earth, that radius would subtend an angle of only $\sim 0.''25$.

Inclusion of the resonant-relaxation diffusion coefficients implies a different steady state. Inside ~ 0.05 pc, the density profile remains much shallower than the Bahcall-Wolf form, with $\rho \sim r^{-0.5}$ – the functional form that corresponds to an f that is fully depleted at high binding energies. The radius of this “core” is consistent with the prediction made above ($\sim 0.01 r_m$) given that $r_m \approx 2.5$ pc.

Since the radius of the core is a function of the density normalization, steady state solutions in the presence of resonant relaxation are expected to depend on (at least) one more parameter than in the classical case. A more general exploration of solutions like these will be presented in Paper II from this series (Merritt 2015a).

I thank A. Hamers for providing data from his TPI code that was used in deriving the functional forms of the RR diffusion coefficients in §3.2, and H. Cohn for helpful discussions. This work was supported by the National Science Foundation under grant no. AST 1211602 and by the National Aeronautics and Space Administration under grant no. NNX13AG92G.

APPENDIX

Numerical Evaluation of the C_i

The functions $C_i(s = \mathcal{E}'/\mathcal{E}, \mathcal{R})$ that appear in equation (27b),

$$F_i(\mathcal{E}, \mathcal{R}) = 4\pi\Gamma \int_{\mathcal{E}}^{\mathcal{E}/x_-} \bar{f}(\mathcal{E}') C_i\left(\frac{\mathcal{E}'}{\mathcal{E}}, \mathcal{R}\right) d\mathcal{E}'$$

are given by Cohn & Kulsrud (1978) as

$$\begin{aligned} C_1 &= \frac{2}{\pi} \int dx Q^{-1/2} \frac{x(1-sx)^{1/2}}{(1-x)^{1/2}}, \\ C_2 &= \frac{2}{\pi} \int dx Q^{-1/2} \frac{x^2(1-sx)^{1/2}}{(1-x)^{3/2}}, \\ C_3 &= \frac{2}{\pi} \int dx Q^{-1/2} \frac{x^3(1-sx)^{1/2}}{(1-x)^{1/2}}, \\ C_4 &= \frac{2}{\pi} \int dx Q^{-1/2} \frac{(1-sx)^{3/2}}{(1-x)^{1/2}}, \\ C_5 &= \frac{2}{\pi} \int dx Q^{-1/2} \frac{x(1-sx)^{3/2}}{(1-x)^{3/2}}, \\ C_6 &= \frac{2}{\pi} \int dx Q^{-1/2} \frac{x^2(1-sx)^{3/2}}{(1-x)^{5/2}}, \\ C_7 &= \frac{2}{\pi} \int dx Q^{-1/2} \frac{x^3(1-sx)^{3/2}}{(1-x)^{3/2}}. \end{aligned} \tag{A1}$$

In these expressions, $Q \equiv (x_+ - x)(x - x_-)$ with $x_{\pm} = (1/2) [1 \pm \sqrt{1 - \mathcal{R}}]$, and the limits of integration are x_- and $\max[x_-, \min(x_+, s^{-1})]$. These functions are independent of f and so can be evaluated on a fixed numerical grid. The grid axes were chosen to be $\{\mathcal{R}, W\}$ where

$$W \equiv \frac{2T - 1 + \sqrt{1 - \mathcal{R}}}{1 + \sqrt{1 - \mathcal{R}}} \tag{A2}$$

and $T \equiv s^{-1} = \mathcal{E}/\mathcal{E}'$. Thus $0 \leq W \leq 1$, $0 \leq \mathcal{R} \leq 1$, and

$$T = \frac{1}{2} \left[1 - \sqrt{1 - \mathcal{R}} + W \left(1 + \sqrt{1 - \mathcal{R}} \right) \right]. \tag{A3}$$

Typically the number of grid points was 256×256 .

The C_i are finite for all $\{\mathcal{R}, W\}$ with the exception of C_2 and C_6 , which diverge at

$$\mathcal{R} = 0, \quad W = T = s = 1. \quad (\text{A4})$$

Along the $\mathcal{R} = 0$ border, both functions diverge as $(1 - W)^{-1/2}$ as $W \rightarrow 1$, while along the $W = 1$ border they diverge as $\mathcal{R}^{-1/2}$ as $\mathcal{R} \rightarrow 0$. To deal with the divergence, C_2 and C_6 were multiplied by the function

$$\left[\mathcal{R}^2 + 256(1 - W)^2 \right]^{1/4} \quad (\text{A5})$$

before storing their computed values on the grid. Integrations were carried out with routine `d01apf` from the *Numerical Algorithms Group* fortran subroutine library. Accuracy of the integrations was checked by comparison with analytic expressions that obtain along the grid boundaries; for instance, for $\mathcal{R} = 1$, $C_i = g_i(s)$ where

$$\begin{aligned} g_1 = g_2 &= \sqrt{2 - s}, & g_3 &= \frac{1}{4}\sqrt{2 - s}, \\ g_4 = g_5 = g_6 &= (2 - s)^{3/2}, & g_7 &= \frac{1}{4}(2 - s)^{3/2}. \end{aligned} \quad (\text{A6})$$

Once the values of the C_i had computed on the $\{\mathcal{R}, W\}$ grid, the NAG routine `e01daf` was used to fit a bicubic interpolating spline to the computed values. During integrations of the Fokker-Planck equation, values of the C_i between the $\{\mathcal{R}, W\}$ grid points were then computed from the spline coefficients.

APPENDIX

$N_r(a)$ vs. $N_a(a)$

This appendix compares two quantities:

1. $N_r(< a)$, the number of stars with instantaneous radii less than a ;
2. $N_a(< a)$, the number of stars with semimajor axes less than a .

A power-law dependence of number density on distance from the SBH is assumed:

$$n(r) = n_0 \left(\frac{r}{r_0} \right)^{-\gamma}, \quad \psi(r) = \frac{GM_\bullet}{r} \quad (\text{B1})$$

so that the number of stars instantaneously below r is

$$N_r(< r) = \frac{4\pi}{3 - \gamma} n_0 r_0^3 \left(\frac{r}{r_0} \right)^{3 - \gamma}. \quad (\text{B2})$$

The distribution function is assumed to be isotropic; Eddington's formula gives

$$f(\mathcal{E}) = f_0 \left(\frac{\mathcal{E}}{\mathcal{E}_0} \right)^\eta, \quad \eta = \gamma - 3/2 \quad (\text{B3a})$$

$$= \frac{1}{(2\pi)^{3/2}} \frac{\Gamma(\gamma + 1)}{\Gamma(\gamma - 1/2)} \frac{n_0 r_0^\gamma}{(GM_\bullet)^{-\gamma}} \mathcal{E}^{\gamma - 3/2}. \quad (\text{B3b})$$

The number of stars per unit of binding energy is

$$N(\mathcal{E})d\mathcal{E} = 4\pi^2 p(\mathcal{E})f(\mathcal{E})d\mathcal{E}, \quad p(\mathcal{E}) = \frac{\sqrt{2}\pi}{4} (GM_\bullet)^3 \mathcal{E}^{-5/2} \quad (\text{B4})$$

so that

$$N(\mathcal{E})d\mathcal{E} = \frac{\pi^{3/2}}{2} \frac{\Gamma(\gamma + 1)}{\Gamma(\gamma - 1/2)} (GM_\bullet)^{3 - \gamma} n_0 r_0^\gamma \mathcal{E}^{\gamma - 4} d\mathcal{E} \quad (\text{B5})$$

and the number of stars with binding energies greater than \mathcal{E} is

$$N_{\mathcal{E}(> \mathcal{E})} = \int_{\mathcal{E}}^{\infty} N(\mathcal{E})d\mathcal{E} = \frac{\pi^{3/2}}{2(3 - \gamma)} \frac{\Gamma(\gamma + 1)}{\Gamma(\gamma - 1/2)} (GM_\bullet)^{3 - \gamma} n_0 r_0^\gamma \mathcal{E}^{\gamma - 3}. \quad (\text{B6})$$

Setting $\mathcal{E} = GM_\bullet/(2a)$ yields the number of stars with semimajor axes less than a :

$$N_a(< a) = \frac{2^{2 - \gamma} \pi^{3/2}}{(3 - \gamma)} \frac{\Gamma(\gamma + 1)}{\Gamma(\gamma - 1/2)} n_0 r_0^3 \left(\frac{a}{r_0} \right)^{3 - \gamma}. \quad (\text{B7})$$

Equations (B2) and (B7) can be written

$$N_r(< a) = N_1(\gamma) n_0 r_0^3 \left(\frac{a}{r_0}\right)^{3-\gamma}, \quad N_a(< a) = N_2(\gamma) n_0 r_0^3 \left(\frac{a}{r_0}\right)^{3-\gamma} \quad (\text{B8})$$

with

$$N_1(\gamma) = \frac{4\pi}{3-\gamma}, \quad N_2(\gamma) = \frac{2^{2-\gamma} \pi^{3/2}}{3-\gamma} \frac{\Gamma(\gamma+1)}{\Gamma(\gamma-1/2)}. \quad (\text{B9})$$

Values of N_1 and N_2 are given in the table. For $\gamma \gtrsim 3/2$ the two quantities are very similar; they begin to depart

γ	1	3/2	7/4	2	5/2
N_1	6.28	8.38	10.05	12.56	25.13
N_2	3.14	6.98	9.40	12.56	26.17
N_2/N_1	0.50	0.83	0.94	1.00	1.04

significantly for smaller γ .

APPENDIX

Anomalous Relaxation

A Monte-Carlo algorithm for describing the evolution of L in the ‘‘anomalous relaxation’’ ($L \lesssim L_{\text{SB}}$) regime was presented in Merritt et al. (2011). That algorithm was based on a simple model for the time- and space-dependence of the \sqrt{N} perturbing potential. Following is an analytic derivation of the angular momentum transition probabilities, and the corresponding diffusion coefficients, that are implied by the same Hamiltonian model. The results of the derivation presented in this appendix were the basis for the functional forms that Hamers, Portegies Zwart & Merritt (2014) fit to diffusion coefficients extracted from their N -body data, and which appear here in §3.3.

Consider a star orbiting in the potential

$$\Phi(\mathbf{r}) = \Phi_{\text{Kepler}} + \Phi_{\text{N}} + \Phi_{\sqrt{N}}. \quad (\text{C1})$$

Here, $\Phi_{\text{Kepler}} = -GM_{\bullet}/r$ is the (Newtonian) potential due to the SBH; Φ_{N} is the potential from the spherically-distributed mass; and $\Phi_{\sqrt{N}}$ is the potential due to the \sqrt{N} asymmetries in the stellar distribution. We assume that $|\Phi_{\sqrt{N}}| \ll |\Phi_{\text{N}}| \ll |\Phi_{\text{Kepler}}|$.

If the mass density falls off as a power of radius, $\rho(r) = \rho_0(r/r_0)^{-\gamma}$, then

$$\Phi_{\text{N}}(r) = \frac{4\pi G \rho_0 r_0^2}{(2-\gamma)(3-\gamma)} \left(\frac{r}{r_0}\right)^{2-\gamma} + \text{constant} \quad (\text{C2})$$

for $\gamma \neq 2$; for $\gamma = 2$ the dependence of Φ_{N} on radius becomes logarithmic. Following Merritt et al. (2011), we assume that the \sqrt{N} perturbing potential, as experienced by a test star of semimajor axis a , is given by

$$\Phi_{\sqrt{N}} = -aS(a) \cos \theta = -aS(a) \frac{z}{r}, \quad S(a) = \frac{Gm_{\star}}{a^2} \sqrt{N(a)}. \quad (\text{C3})$$

We are assuming for the moment that $\Phi_{\sqrt{N}}$ is independent of time. Expressing the two perturbing potentials in Delaunay variables and averaging over the unperturbed (Keplerian) motion yields

$$\overline{\Phi_{\text{N}}} = \frac{GM_{\star}(r < a)}{(2-\gamma)a} (1 + \alpha_1 - \alpha_2 \ell^2), \quad (\text{C4a})$$

$$\overline{\Phi_{\sqrt{N}}} = aS(a) e \sin i \sin \omega. \quad (\text{C4b})$$

Here, $\ell \equiv \sqrt{1-e^2}$, $i = \pi/2$ corresponds to the $x-z$ plane and $\omega = \pi/2$ describes an orbit that is elongated along z . The expression for $\overline{\Phi_{\text{N}}}$ assumes $\ell \ll 1$; the quantities $\alpha_1(\gamma)$, $\alpha_2(\gamma)$ are both of order unity and are given in Merritt (2013, §4.4.1).

Ignoring constant terms (including terms that depend only on a), the averaged Hamiltonian is then

$$H \equiv \frac{\overline{\Phi}}{\nu_0 I} = -\ell^{-1} - A_{\text{N}} \ell^2 + A_{\sqrt{N}} e \sin i \sin \omega, \quad (\text{C5a})$$

$$A_{\text{N}} = \frac{\alpha_2}{3(2-\gamma)} \frac{M_{\star}(a)}{M_{\bullet}} \frac{a}{r_g}, \quad A_{\sqrt{N}} = \frac{1}{2} \frac{S(a)}{GM_{\bullet}/a^2} \frac{a}{r_g} \quad (\text{C5b})$$

and

$$r_g \equiv \frac{GM_\bullet}{c^2}, \quad \nu_0 = \frac{2\pi}{P(a)} \frac{3r_g}{a}, \quad I = (GM_\bullet a)^{1/2}. \quad (\text{C6})$$

Discarding terms of order ℓ^2 or smaller, the averaged Hamiltonian becomes

$$H = -\ell^{-1} + A\sqrt{N} \sin i \sin \omega. \quad (\text{C7})$$

Note that the ‘‘mass precession’’ terms vanishes to this order in ℓ . The first term in equation (C7) represents GR precession; the second represents the effects of the \sqrt{N} torques.

Writing $\tau = \nu_0 t$, Hamilton’s equations of motion for the osculating elements are

$$\begin{aligned} \frac{d\omega}{d\tau} &= \frac{\partial H}{\partial \tau} = \ell^{-2}, & \frac{d\ell}{d\tau} &= -\frac{\partial H}{\partial \omega} = -A\sqrt{N} \sin i \cos \omega, \\ \frac{d\Omega}{d\tau} &= \frac{\partial H}{\partial \ell_z} = -A\sqrt{N} \frac{\ell_z \sin \omega}{\ell^2 \sin i}, & \frac{d\ell_z}{d\tau} &= 0. \end{aligned} \quad (\text{C8})$$

Henceforth setting $\sin i = 1$, the dependence of ℓ on ω is given by

$$\ell^{-1} = \frac{1}{2\ell_1 \ell_2} [(\ell_2 - \ell_1) \sin \omega + (\ell_1 + \ell_2)] \quad (\text{C9a})$$

$$= A\sqrt{N} (\sin \omega + g_0) \quad (\text{C9b})$$

where $\{\ell_1, \ell_2\}$ are the extreme values of ℓ and $g_0 = -H/A\sqrt{N}$ is the ‘‘energy.’’ The equation of motion for ℓ can be expressed in terms of ℓ alone as

$$\frac{d\ell}{d\tau} = \pm \sqrt{\left(\frac{1}{\ell_1} - \frac{1}{\ell}\right) \left(\frac{1}{\ell} - \frac{1}{\ell_2}\right)}, \quad (\text{C10})$$

with a similar expression for $\dot{\omega}$, and the full precessional period is

$$T_0 = \frac{2\pi}{A^2 \sqrt{N}} \frac{g_0}{(g_0^2 - 1)^{3/2}} \quad (\text{C11})$$

where

$$\ell_1 = A\sqrt{N}^{-1} (g_0 + 1)^{-1}, \quad \ell_2 = A\sqrt{N}^{-1} (g_0 - 1)^{-1}; \quad (\text{C12})$$

thus $g_0 = (\ell_2 + \ell_1)/(\ell_2 - \ell_1)$ and

$$\frac{\ell_1 + \ell_2}{2} \equiv \ell_{\text{av}} = \frac{1}{A\sqrt{N}} \frac{g_0}{g_0^2 - 1}. \quad (\text{C13})$$

Solutions obtained so far describe ‘‘coherent resonant relaxation:’’ changes in a star’s angular momentum for times shorter than the coherence time. Now, suppose that the orientation of the torquing potential changes, instantaneously, at random times separated by t_{coh} . Of course this is a crude oversimplification since in reality the torquing potential is changing gradually; on the other hand, for stars near the Schwarzschild barrier, the GR precession time is expected to be comparable to the coherence time (equation 68).

Let the angle between the new z -axis, and the orbital semimajor axis at the moment of the switch, be ω_1 . At this moment, ℓ has the value ℓ_s , and g_0 changes to g_1 , where

$$g_1 = 1/(A\sqrt{N}\ell_s) - \sin \omega_1. \quad (\text{C14})$$

Since the probability distributions of τ and ω_1 are uniform, we can write

$$P(\ell_s, g_1) d\ell_s dg_1 = P(\tau, \omega_1) d\tau d\omega_1 = \frac{4}{2\pi T_0}. \quad (\text{C15})$$

The factor four on the RHS accounts for the fact that ℓ varies over its full range in one-fourth of a precessional period. Then

$$P(\ell_s, g_1) = \frac{2}{\pi T_0} \frac{\partial(\tau, \omega_1)}{\partial(\ell_s, g_1)} \equiv \frac{2}{\pi T_0} J, \quad (\text{C16a})$$

$$J^{-1} = \frac{\partial(\ell_s, g_1)}{\partial(\tau, \omega_1)} = \left| \frac{d\ell_s}{d\tau} \frac{\partial g_1}{\partial \omega_1} \right|, \quad (\text{C16b})$$

$$J = A\sqrt{N} \sqrt{1 - [g_0 - 1/(A\sqrt{N}\ell_s)]^2} \sqrt{1 - [g_1 - 1/(A\sqrt{N}\ell_s)]^2}. \quad (\text{C16c})$$

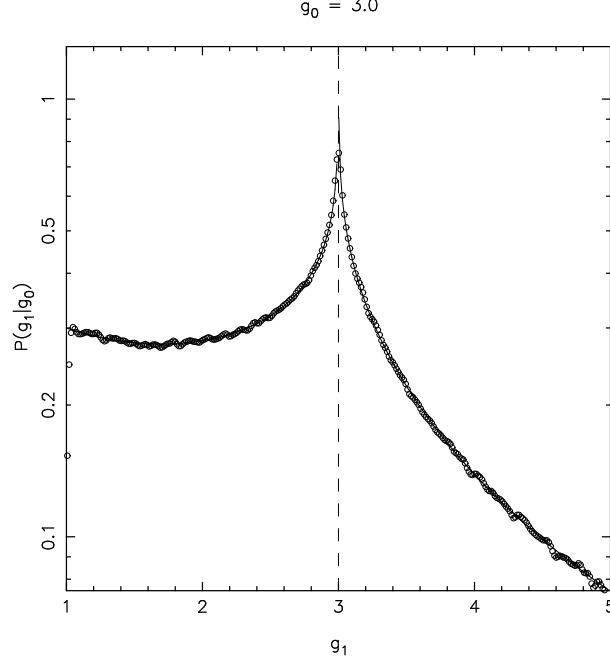


FIG. 10.— $P(g_1|g_0)$ computed in two ways, for $g_0 = 3$.

Integrating over ℓ_s gives the probability distribution for g_1 . This can be written

$$P(g_1|g_0) = \frac{2}{\pi T_0 A^2 \sqrt{N}} \int_{x_1}^{x_2} \frac{dx}{x^2 \sqrt{(x-x_1)(x_2-x)[2-(x-x_1)][2-(x_2-x)]}} \quad (\text{C17})$$

where

$$x_1 = g_0 - 1, \quad x_2 = g_1 + 1 \quad (\text{C18})$$

for $g_1 < g_0$, and

$$x_1 = g_1 - 1, \quad x_2 = g_0 + 1 \quad (\text{C19})$$

for $g_1 > g_0$. Figure 10 shows a numerical integration of equation (C17) (solid line) for $g_0 = 3$, compared with the results of Monte-Carlo experiments based on the equations of motion (C8). We note here the asymmetry of the derived transition probability.

The diffusion coefficients are

$$\langle (\Delta g_0)^k \rangle = \frac{1}{T_{\text{coh}}} \int_{g_0-2}^{g_0+2} (g_1 - g_0)^k P(g_1|g_0) dg_1. \quad (\text{C20})$$

The integral (C20) can be broken into two pieces, $I_>$ and $I_<$, corresponding to $g_0 > g_1$ and $g_0 < g_1$ respectively. In the case of $\langle \Delta g_0 \rangle$,

$$\left(\frac{\pi}{2} T_0 A^2 \sqrt{N} T_{\text{coh}} \right) I_> = \int_{x_1}^{x_1+2} (x_2 - x_1 - 2) dx_2 \int_{x_1}^{x_2} \frac{dx}{x^2 \sqrt{(x_2-x)(x-x_1)[2-(x_2-x)][2-(x-x_1)]}} \quad (\text{C21a})$$

$$= -\frac{2}{g_0^2 - 1} - 2 \int_0^2 \frac{(1-w)dw}{\sqrt{w(2-w)}(w+g_0-1)^2} \sin^{-1} \sqrt{\frac{2-w}{2}} \quad (\text{C21b})$$

and a similar calculation gives

$$\left(\frac{\pi}{2} T_0 A^2 \sqrt{N} T_{\text{coh}} \right) I_< = \frac{2}{g_0^2 - 1} + 2 \int_0^2 \frac{(1-w)dw}{\sqrt{w(2-w)}(-w+g_0+1)^2} \sin^{-1} \sqrt{\frac{2-w}{2}}. \quad (\text{C22})$$

The sum is

$$\left(\frac{\pi}{2} T_0 A^2 \sqrt{N} T_{\text{coh}} \right) (I_< + I_>) = -\frac{8}{g_0^3} I(g_0), \quad (\text{C23a})$$

$$I(g_0) = \int_{-1}^1 \frac{x^2 dx}{(g_0^2 - x^2)^2 \sqrt{1-x^2}} \sin^{-1} \sqrt{\frac{1-x}{2}} = \frac{\pi^2}{8} \frac{g_0^3}{(g_0^2 - 1)^{3/2}}. \quad (\text{C23b})$$

Thus

$$\langle \Delta g_0 \rangle = -\frac{8}{g_0^3} \frac{2}{\pi T_{\text{coh}} T_0 A^2 \sqrt{N}} I(g_0) = -\frac{1}{t_{\text{coh}}} \frac{1}{g_0}. \quad (\text{C24})$$

Proceeding as before to evaluate $\langle (\Delta g_0)^2 \rangle$:

$$\begin{aligned} \langle (\Delta g_0)^2 \rangle &= \frac{2}{\pi T_0 A^2 \sqrt{N} T_{\text{coh}}} (I_{<} + I_{>}) = \frac{1}{T_{\text{coh}}} K(g_0), \\ K(g_0) &= \left[\frac{5}{2} + \frac{(g_0^2 - 1)^{3/2}}{g_0} - g_0^2 \right]. \end{aligned} \quad (\text{C25})$$

The function $K(g_0)$ is almost independent of g_0 :

$$K(3) = 1.042, \quad K(5) = 1.015, \quad K(8) = 1.006, \quad K(10) = 1.004, \quad K(20) = 1.001, \quad K(\infty) = 1$$

so that

$$\langle (\Delta g_0)^2 \rangle = (1.0_{-0}^{+0.042}) \frac{1}{t_{\text{coh}}}. \quad (\text{C26})$$

To a good approximation then,

$$\langle \Delta g_0 \rangle = -\frac{1}{t_{\text{coh}}} \frac{1}{g_0}, \quad \langle (\Delta g_0)^2 \rangle = \frac{1}{t_{\text{coh}}} \quad (\text{C27})$$

and the time scales for changes in g_0 are

$$\left| \frac{\langle \Delta g_0 \rangle}{g_0} \right|^{-1} \approx \left| \frac{\langle (\Delta g_0)^2 \rangle}{g_0^2} \right|^{-1} \approx g_0^2 t_{\text{coh}}. \quad (\text{C28})$$

Identifying ℓ with ℓ_{av} (equation C13), diffusion coefficients in ℓ become

$$\langle \Delta \ell \rangle \approx \frac{2\ell^3}{\tau} \left[1 + \frac{3}{2} (A\sqrt{N} \ell)^2 \right], \quad (\text{C29a})$$

$$\langle (\Delta \ell)^2 \rangle \approx \frac{\ell^4}{\tau} \left[1 + 2 (A\sqrt{N} \ell)^2 \right] \quad (\text{C29b})$$

where $\tau(a) \equiv t_{\text{coh}}(a)/(A\sqrt{N})^2$.

REFERENCES

- Bahcall, J. & Wolf, S. 1976, ApJ, 209, 214
 Cohn, H. & Kulsrud, R. 1978, ApJ, 226, 1087
 Dale, J. E., Davies, M. B., Church, R. P., & Freitag, M. 2009, MNRAS, 393, 1016
 Eilon, E., Kupi, G., & Alexander, T. 2009, ApJ, 698, 641
 Frank, J. & Rees, M. J. 1976, MNRAS, 176, 633
 Hamers, A., Portegies Zwart, S. & Merritt, D. 2014, MNRAS, 443, 355
 Hopman, C., & Alexander, T. 2006, ApJ, 645, L133
 Lightman, A. P. & Shapiro, S. L. 1977, ApJ, 211, 244
 MacLeod, M., Guillochon, J., & Ramirez-Ruiz, E. 2012, ApJ, 757, 134
 Madigan, A.-M., Hopman, C., & Levin, Y. 2011, ApJ, 738, 99
 Magorrian, J. & Tremaine, S. 1998, MNRAS, 309, 447.
 Merritt, D. 2010, ApJ, 718, 739
 Merritt, D. 2013, Dynamics and Evolution of Galactic Nuclei (Princeton: Princeton University Press).
 Merritt, D. 2015, ApJ, 804, 128
 Merritt, D. 2015, ApJ, submitted
 Merritt, D., Alexander, T., Mikkola, S., & Will, C. M. 2011, PhRv, 84, 044024
 Rauch, K. P., & Tremaine, S. 1996, NewA, 1, 149
 Rosenbluth, M. N., MacDonald, W. M., & Judd, D. L. 1957, PhRv, 107, 1
 Schödel, R., Merritt, D., & Eckart, A. 2009, A&A, 502, 91